



**SPE 138366**

## **The Influence of Wettability on Oil Recovery From Naturally Fractured Oil Reservoirs Including Non-Equilibrium Effects**

H. Salimi and J. Bruining, Delft University of Technology

Copyright 2010, Society of Petroleum Engineers

This paper was prepared for presentation at the SPE Latin American & Caribbean Petroleum Engineering Conference held in Lima, Peru, 1–3 December 2010.

This paper was selected for presentation by an SPE program committee following review of information contained in an abstract submitted by the author(s). Contents of the paper have not been reviewed by the Society of Petroleum Engineers and are subject to correction by the author(s). The material does not necessarily reflect any position of the Society of Petroleum Engineers, its officers, or members. Electronic reproduction, distribution, or storage of any part of this paper without the written consent of the Society of Petroleum Engineers is prohibited. Permission to reproduce in print is restricted to an abstract of not more than 300 words; illustrations may not be copied. The abstract must contain conspicuous acknowledgment of SPE copyright.

### **Abstract**

In the laboratory, partially water-wet systems are often mistaken for completely oil-wet systems, because imbibition only starts after removal of the oil layer, which originally covers the grains. The (long) time required to remove the oil film will be referred to as delay time. Incorporation of delay time in a more general description of capillary pressure and relative permeability functions is called the non-equilibrium effect. No attempt has yet been made to model non-equilibrium effects in fractured reservoirs for a field-scale problem and this is the main innovative aspect of this paper. We apply homogenization to derive an upscaled model for fractured reservoirs and include delay time effects. Furthermore, we develop a computationally efficient numerical approach to solve the upscaled model. The upscaled model overcomes limitations of the dual-porosity model including the use of a transfer function and shape factor. This paper examines various aspects of wettability behavior in fractured reservoirs, viz., the contact angle, mixed wetting, and non-equilibrium effects in capillary pressure. The main characteristic that determines reservoir behavior is the Peclet number that expresses the ratio of the average imbibition time divided by the residence time of the fluids in the fractures.

At low Peclet numbers and thus high gravity numbers, under-riding is aggravated by large contact angles and longer delay times. However, for low Peclet and low gravity numbers, the effect of contact angle and delay time for the non-equilibrium effects can be ignored without appreciable loss of accuracy. For low Peclet numbers, the recovery for the mixed-wet fracture/mixed-wet matrix case is more than for the water-wet fracture/mixed-wet matrix case because a combination of capillary imbibition and gravity drainage occurs in the former case. For low Peclet numbers, the ultimate oil recovery for the water-wet fracture/mixed-wet matrix case is about the matrix Amott index times the recovery obtained for completely water-wet reservoirs. For residence times of water in the fractured reservoir much longer than the delay time, the delay time (non-equilibrium effect) does not influence the oil recovery qualitatively. Conversely, for high Peclet numbers, the residence time of water in the fractures is short and the relatively longer delay times reduce the cumulative oil production considerably as expected. Furthermore, at high Peclet numbers, after water breakthrough, the oil recovery appears to be approximately proportional to the cosine of the contact angle. It is important to distinguish between truly oil-wet systems and systems that are water-wet with long delay times. The efficiency of waterflooding in naturally fractured oil reservoirs decreases in the sequence of completely water-wet, mixed-wet fracture/mixed-wet matrix, water-wet fracture/mixed-wet matrix, and completely oil-wet, respectively. For the same amount of injected water, the recovery at low Peclet numbers is larger than the recovery at high Peclet numbers.

### **Introduction**

Fractured hydrocarbon reservoirs provide over 20% of the world's oil reserves and production (Saidi 1983; Firoozabadi 2000). Virtually, all reservoirs contain at least some natural fractures (Aguilera 1998; Nelson 2001). However, from the reservoir modeling point of view, a fractured reservoir is defined as a reservoir in which naturally occurring fractures have a significant effect on fluid flow (Salimi and Bruining 2008, 2010a, 2010b). We only consider reservoirs where fluid flow occurs predominantly in a connected fracture network and do not consider the case of limited connectivity and for the case that fractures act as a barrier for fluid flow. Fractured-reservoir simulations completely differ from conventional-reservoir simulations. The challenge of upscaling is to give an accurate representation of the interaction between fractures and matrix blocks. This is because the fracture-matrix interaction leads to a delayed response that distinguishes the flow through fractured reservoirs from the flow through heterogeneous single-porosity reservoirs (Wu et al. 2004; Salimi and Bruining 2009, 2010a).

Many geological situations lead to some type of fractured reservoirs (Aguilera 1998; Nelson 2001). From the geological point of view, fractured reservoirs can exhibit a number of topologically different configurations. These are reservoirs built

from (1) matrix blocks that are bounded by fracture planes in all directions (totally fractured reservoirs, TFRs, or sugar cube) (Salimi and Bruining 2010a), (2) matrix blocks that are bounded only by more or less vertical fracture planes (vertically fractured reservoirs, VFRs) (Salimi and Bruining 2010b), and (3) matrix blocks that form a connected domain interdispersed with fractures (partially fractured reservoirs, PFRs) (Salimi and Bruining 2009). Matrix blocks in the sugar-cube configuration are pressed against each other, and consequently contact regions are usually crushed and impermeable except in shallow hydrology applications (Dahan et al. 1998; Zanini et al. 2000). It has been argued that the sugar-cube configuration is unrealistic at large depth, because the horizontal fractures will close due to the overburden pressure. This ignores the possibility that two fracture sets are oblique leading to horizontal columns. If these columns are intersected by a third perpendicular fracture set, matrix blocks can occur that are bounded by three fracture planes (Finkbeiner et al. 1997; Teixell et al. 2000). In the VFR configuration, the top and bottom of the columns are bounded by the impermeable cap- and base-rock. From the geological perspective, a VFR is more abundant than a sugar-cube configuration because in the most important natural fractures for oil recovery and oil reservoirs, i.e., regional and tectonic, fracture planes are perpendicular to the bedding planes. Therefore, the upscaled-VFR model would be appropriate for these types of fractures. A VFR cannot be mimicked with a sugar-cube model in which the horizontal fracture is very small because it precludes capillary continuity of stacked matrix blocks. It is also not mimicked by a zero width horizontal fracture because such a fracture will act like a barrier and impedes vertical flow.

The current literature in the petroleum community dealing with flow in fractured reservoirs is largely confined to topological equivalents of the sugar-cube model, i.e., the matrix blocks are surrounded by fractures from all sides (Barenblatt et al. 1960; Warren and Root 1963; Kazemi 1969; Sonier et al. 1988; Kazemi et al. 1992; Al-Huthali and Datta-Gupta 2004; Al-Harbi et al. 2005; Sarma and Aziz 2006). However, the VFR (aggregated-column) model is topologically different because it is not connected to the fracture network through the top and bottom of the matrix column. Moreover, in a VFR configuration, there is no separation of scales in the vertical direction because the global scale is the same as the local scale. In this case, only upscaling in a plane perpendicular to the columns is required. As a result, the global (effective) fracture permeability and the fluid-flow exchange term in the upscaled model for the VFR configuration become different from those for sugar-cube configuration. To our knowledge, the current reservoir simulators have no option to deal with this situation and this is one innovative aspect of this contribution. The novel feature of the upscaled-VFR model is that, for example, fracture fluid may enter the matrix column at one height, travel downward for some time, and then re-enter the fractures at a lower height. Indeed, the physics of the upscaled-VFR model is different from the physics of the sugar-cube model. The main reason is that gravity plays a more important role, meaning that gravity and capillary phenomena interact in the matrix columns.

We apply homogenization to derive an upscaled model for vertically fractured reservoirs, as proposed by Douglas (Douglas et al. 1991) and Arbogast (1993). It has several advantages over the transfer-function and shape-factor approach. Homogenization is rigorous in the sense that no prerequisites are imposed on the upscaled (macroscopic) models (Auriault and Lewandowska 1996). It explicitly shows the dependence of the upscaled equations on the characteristic dimensionless numbers of interest. However, homogenization still uses a number of assumptions for the physics of flow in porous media (e.g., separation of scales, periodic boundary conditions). A full overview of simplifications and assumptions needed for the aggregated columns to justify the upscaling procedure can be found in Salimi and Bruining (2010b).

In fractured reservoirs, capillary forces, leading to counter-current or co-current imbibition (Pooladi-Darvish and Firoozabadi 2000; Rangel-German and Kovscek 2002; Behbahani and Blunt 2005; Hatiboglu and Babadagli 2007; Karimaie and Torsæter 2007), are the main drivers for waterdrive recovery from the matrix blocks (Firoozabadi 2000). Reservoir wettability and its effect on oil recovery have been the subject of numerous studies (Anderson 1987; Tang and Firoozabadi 2001; Morrow and Mason 2001; Graue et al. 2001; Seethepalli et al. 2004). However, these studies address drainage and imbibition behavior on a laboratory scale, which describe only one facet for multiphase flow in fractured reservoirs. Therefore, major issues of oil recovery related to wettability at a full-field reservoir scale remain poorly understood. One of the major parameters of wettability is the contact angle (Tartakovsky and Meakin 2005). Monteagudo and Firoozabadi (2007) extended the control-volume discrete-fracture model to incorporate matrix heterogeneity and reservoir wettability effects. The discrete fracture approach differs from the homogenization approach, but also does not use semi-empirical transfer functions. Delshad et al. (2009) modeled chemical processes leading to wettability alteration in naturally fractured reservoirs using UTCHEM and validated the proposed wettability-alteration model against laboratory experiments. Although capillary forces are the dominant driving forces for spontaneous imbibition, the rate of imbibition depends on many factors, e.g., fluid viscosity and matrix-block size. Tong et al. (2002), Fischer and Morrow (2006), and Fischer et al. (2008) have investigated the effect of viscosity ratio on spontaneous imbibition by performing laboratory experiments and verifying data by a model.

Experimental evidence (Topp et al. 1967; Smiles et al. 1971; Vachaud et al. 1972; Elzeftawy and Mansell 1975; Stauffer 1978; Tang and Firoozabadi 2001; Siemons et al. 2006; Plug and Bruining 2007; Plug et al. 2008; Yu et al. 2009) supports a more general description of capillary-pressure and relative-permeability functions that include the non-equilibrium effect. Reservoir interpretation that does not recognize the potential for reduced recovery because of non-equilibrium effects may lead to an incorrect estimation of the recovery. The concept of the non-equilibrium effect was first introduced by Barenblatt and his colleagues (Barenblatt 1971; Barenblatt and Gilman 1987; Barenblatt et al. 1997, 2003). It is equivalent to an alternative formulation introduced by Hassanizadeh and Gray (1990, 1993) and Pavone (1990). We follow the formulation by Barenblatt, because it has been worked out for both the capillary-pressure and relative-permeability functions. To our knowledge, this problem has not been discussed previously for a field-scale problem and this is another innovative aspect of this paper. To

examine whether the non-equilibrium effect has any effect on larger-scale problems, we construct an upscaled model in which the non-equilibrium effects are included. We use the simulation to determine the range of delay times to investigate whether discernable effects occur in terms of oil recovery.

The objective of this paper is to investigate wettability aspects of fractured reservoirs; to illustrate that the ensuing upscaled equations are able to deal with all wettability aspects of fractured-reservoir flow; to develop an efficient fully implicit numerical method for solving the upscaled equations; and to quantify conditions for which non-equilibrium effects in capillary pressure and relative permeabilities determines the recovery behavior.

The paper is organized as follows. First, we briefly describe the physical model and the topological configuration for vertically fractured reservoirs. Next, we explain the theory of non-equilibrium effects in two-phase flow and various wetting conditions. Thirdly, we explain the upscaled model. After that, we introduce the Peclet number to distinguish two different regimes and consider the effect of gravity. Then, we provide numerical simulations at field scale to study the mechanisms mentioned above. Finally, we summarize our findings in the conclusions Section. In Appendix A, we derive the fully implicit numerical scheme.

## Physical Model

In this paper, we extend our previous work (Salimi and Bruining 2009, 2010a, 2010b) on upscaling waterdrive recovery in fractured reservoirs to include non-equilibrium effect in capillary pressures and relative permeabilities. For reasons of easy reference, we shortly repeat the theory for obtaining the upscaled equations.

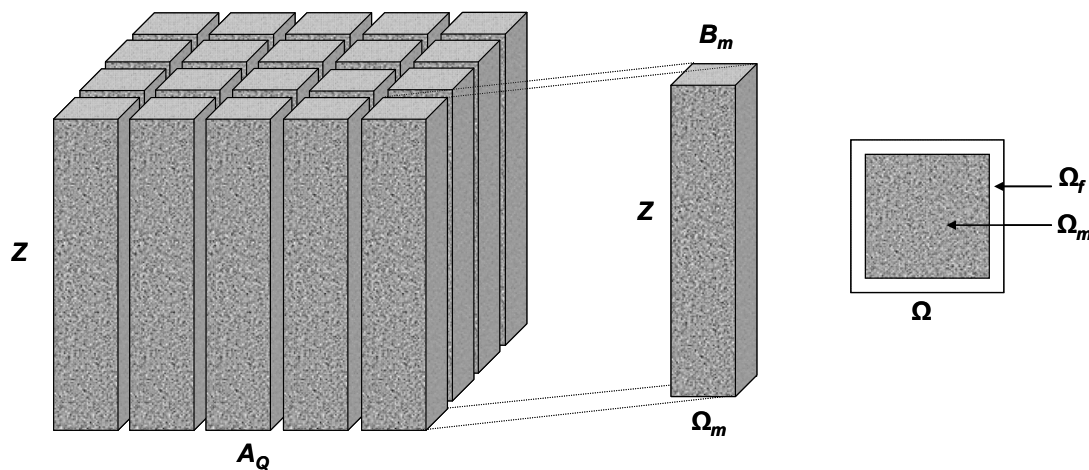


**Fig. 1**—Vertically fractured network (left), matrix column (middle), and horizontal cross section (right) of a small unit that consists of a matrix part and fracture part.

We consider a vertically fractured network (**Fig. 1**) in the domain  $Q = A_Q \times Z$ , where  $A_Q = \{x, y \in \mathbb{R} \mid 0 \leq x \leq L, 0 \leq y \leq W\}$  and  $Z = \{z \in \mathbb{R} \mid 0 \leq z \leq H\}$ , where  $\mathbb{R}$  represents the set of real numbers. We use  $L$ ,  $W$ , and  $H$  to denote the length, width and height of the fractured reservoir. There are two mutually perpendicular vertical fracture sets  $F_1, F_2$ , which surround the matrix column  $B_m = \Omega_m \times Z$ , where  $\Omega_m$  (see Fig. 1) denotes the domain of a horizontal cross-section of a matrix column. Therefore, matrix columns are connected from the top to the bottom of the reservoir domain and there is no direct horizontal fracture connection between matrix columns. Thus, the matrix columns can capture phase segregation caused by gravity. Half of the fracture space surrounding the matrix columns occupy the domain  $B_f = \Omega_f \times Z$ . Furthermore,  $B = \Omega \times Z$  denotes the small periodic units that occupy the domain  $B = B_f \cup B_m$ . All the small units together constitute the VFR.

We simulate the injection of water into a vertically fractured oil reservoir. We apply continuity of capillary pressure and continuity of fluid flow as boundary conditions on the vertical interfaces between fracture and matrix columns. Flux continuity follows from fluid conservation at the interface between fracture and matrix. There is capillary pressure continuity at the boundary of fractures and matrix columns unless one of the phases either in the matrix or in fracture is immobile (Van Duijn et al. 1995). Indeed when one of the phases is immobile, the pressure of that phase depends on local conditions and cannot be determined globally. Hence, the capillary pressure, which is the difference between the phase pressure of the non-wetting phase and wetting phase, can be discontinuous. However, as residual saturations do not flow, this presents no difficulties for the modeling. Continuity of force, and hence continuity of phase pressures, implies continuity of capillary pressure when both phases are mobile.

Moreover, we incorporate the gravity effect directly inside the matrix columns. As a result, there is a net flow within the matrix columns. The symmetry of the fracture pattern in the horizontal plane is such that the fracture permeability can be considered isotropic. We only consider two-phase (oil and water) incompressible flow where the water viscosity,  $\mu_w$ , and the oil viscosity,  $\mu_o$ , are assumed to be constant.

### Model Equations

We use the two-phase ( $\alpha = o, w$ ) extension of Darcy's law for constant fluid densities

$$\begin{aligned}\mathbf{u}_{\alpha f}^* &= -\frac{k_f^* k_{ra,\alpha f}}{\mu_{\alpha f}} \nabla (P_{\alpha f} + \rho_{\alpha} g z) := -\lambda_{\alpha f}^* \nabla \Phi_{\alpha f}, \\ \mathbf{u}_{\alpha m} &= -\frac{k_m k_{ra,\alpha m}}{\mu_{\alpha m}} \nabla \Phi_{\alpha m} := -\lambda_{\alpha m} \nabla \Phi_{\alpha m}.\end{aligned}\quad (1)$$

In these equations, the superscript (\*) denotes the intrinsic (local) fracture properties. The intrinsic fracture permeability evaluated inside the fracture is denoted by  $k_f^*$ . We define the intrinsic fracture permeability  $k_f^*$  based on the fracture aperture. The matrix permeability is denoted by  $k_m$ . Relative permeabilities are denoted by  $k_{rw,\zeta}$  and  $k_{ro,\zeta}$ , where  $\zeta = f, m$  indicates the fracture or matrix systems. Here  $P$  is the pressure,  $\rho$  is the fluid density,  $g$  is the gravity acceleration factor and  $z$  is the vertical upward direction. We define a phase mobility  $\lambda_{\alpha} = k \times k_{ra} / \mu_{\alpha}$  as the ratio between the phase permeability and fluid viscosity. The phase potential  $\Phi_{\alpha}$  is equal to the pressure plus the gravity term.

The mass conservation equation reads

$$\frac{\partial}{\partial t} (\varphi_{\zeta} \rho_{\alpha \zeta} S_{\alpha \zeta}) + \nabla \cdot (\mathbf{u}_{\alpha \zeta} \rho_{\alpha \zeta}) = 0, \quad (2)$$

where  $\varphi$  is the porosity and  $S_{\alpha}$  is the phase saturation. We obtain the governing equations describing incompressible two-phase flow by combining Darcy's Law (Eq. 1) and the mass conservation (Eq. 2)

$$\frac{\partial}{\partial t} (\varphi_f^* \rho_{\alpha f} S_{\alpha f}) = \nabla \cdot (\rho_{\alpha f} \lambda_{\alpha f}^* \nabla \Phi_{\alpha f}) \quad \text{in } \Omega_f, \quad (3)$$

$$\frac{\partial}{\partial t} (\varphi_m \rho_{\alpha m} S_{\alpha m}) = \nabla \cdot (\rho_{\alpha m} \lambda_{\alpha m} \nabla \Phi_{\alpha m}) \quad \text{in } \Omega_m. \quad (4)$$

We define a capillary pressure  $P_c = P_o - P_w$ . This capillary pressure is at equilibrium. At the interface between the fracture and matrix systems, there is continuity of water and oil flow

$$(\rho_{\alpha f} \lambda_{\alpha f}^* \nabla \Phi_{\alpha f}) \cdot \mathbf{n} = (\rho_{\alpha m} \lambda_{\alpha m} \nabla \Phi_{\alpha m}) \cdot \mathbf{n} \quad \text{on } \partial \Omega_m, \quad (5)$$

where  $\mathbf{n}$  denotes the outward unit normal vector to the surface ( $\partial \Omega_m$ ) pointing from the matrix to the fracture. At the interface, there is also continuity of capillary pressure (Van Duijn et al. 1995). Whenever the capillary-pressure function (curve) would be different for two media that are connected with an interface, continuity of capillary pressure results in a discontinuity in saturation. That is the case for fracture-matrix interface since the fracture capillary pressure is smaller than the matrix capillary pressure due to the huge contrast between the intrinsic fracture and matrix permeability. For matrix blocks that are connected to more than one fracture, there is more than one fracture-matrix interface. Consequently, each fracture-matrix interface has its own state of continuity of capillary pressure. If matrix blocks have different flow functions (i.e., capillary-pressure function), continuity of capillary pressure leads to different discontinuities of saturation for each matrix block accordingly (Salimi and Bruining 2010c).

### Contact Angle Effects

Here, we explain the case that the matrix is not completely water-wet ( $0 < \cos \theta < 1$ ). To quantify the effect of contact angle in water-wet VFRs, we assume that the capillary pressure in the matrix system can be given by using the Leverett  $J$ -function (Leverett 1939; Anderson 1987)

$$P_c = \sigma_{wo} \cos \theta \sqrt{\frac{\varphi}{k}} J(S_w). \quad (6)$$

Here,  $\sigma_{wo}$  is the oil-water interfacial tension, and the contact angle  $\theta$  depends on the rock and the two fluids. For a water-wet surface,  $\theta < 90^\circ$ . For an oil-wet (a non-polar surface),  $\theta > 90^\circ$ . Note that it is physically possible for ( $\sigma_{so} - \sigma_{sw} > \sigma_{ow}$ ) and the water would spontaneously spread across the surface. The effect of contact angle on the shape of the capillary-pressure curve is shown in **Fig. 2**.

### Mixed-Wet Effects

Clean rocks, sandy aquifers and surface soils with a low organic content are usually water-wet. Reservoir rocks and surface soils with high organic content are often mixed-wet rather than completely water-wet, i.e., some of the pores are water-wet and others are oil-wet.

As mentioned above, a porous material can be defined as water-wet, oil-wet or mixed-wet. The type of wetting is usually quantified by considering the capillary-pressure curve. There are a number of different indices in use, but we prefer the Amott index to represent the degree of wettability. With reference to **Fig. 3**, the Amott index is

$$I_w = \frac{\Delta S_{ws}}{1 - S_{wc} - S_{or}}, \quad (7)$$

where  $\Delta S_{ws}$  is the difference between the saturation where the capillary-pressure curve crosses the  $P_c = 0$  line and the connate water saturation. For completely water-wet materials,  $I_w = 1$ . If the material is strongly oil-wet,  $I_w = 0$ .

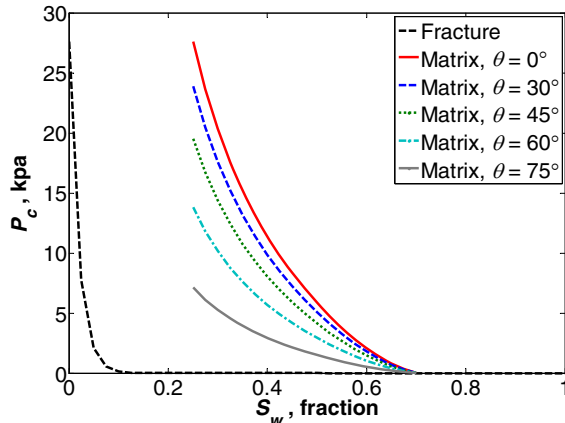


**Fig. 2—Effect of contact angle on the capillary-pressure curves.**

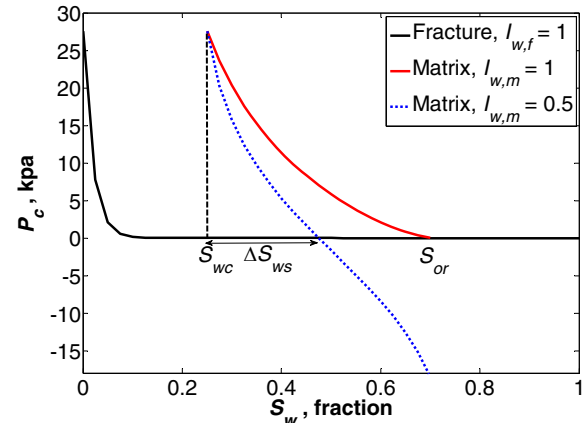


**Fig. 3—Capillary-pressure curve used to determine the Amott index from  $\Delta S_{ws}$  (Eq. 7).**

Note that in Fig. 3, the fracture system is still water-wet. As we see later, when the fracture is also mixed and or oil-wet, the negative part of the capillary pressure given capillary-pressure continuity at the fracture-matrix interface could establish conditions for efficient water-injection processes in mixed-wet fractured reservoirs. This occurs when the capillary pressure ( $P_o - P_w$ ) becomes sufficiently negative. The efficiency therefore depends on the shape of the fracture and the matrix capillary pressure. For favorable capillary-pressure curves, water could be expelled from the fracture and forced into the matrix and consequently water injection in mixed wet fractured reservoirs may be very efficient (Tang and Firoozabadi 2001).

### Non-Equilibrium Effects

The classical two-phase flow model proposed by Muskat and Meres (1936), and Leverett (1939) is based upon the fundamental assumption that the local state of the flow is in equilibrium. This means that the two-phase functions  $k_{rw}$ ,  $k_{ro}$ , and Leverett  $J$ -function are only functions of the water saturation  $S_w$ , independent of whether the water saturation decreases or increases. Therefore, at local equilibrium we have

$$k_{rw} = k_{rw}(S_w), \quad k_{ro} = k_{ro}(S_w), \quad P_c(S_w) = \sigma_{wo} \sqrt{\frac{\phi}{k}} J(S_w), \quad (8)$$

where  $\sigma_{wo}$  is the oil-water interfacial surface tension coefficient, and  $\phi$  and  $k$  are, respectively, the porosity and the absolute permeability of the rock. The dimensionless Leverett  $J$ -function is often assumed to be independent of the porosity and permeability for a specific litho-type.

For increasing (wetting) water saturation, the wetting phase will flow initially in the larger pores, but when steady state ( $\partial S_w / \partial t = 0$ ) is attained it withdraws in the narrower pores and corners and Eq. 8 becomes applicable. There are two reasons that water flows in the larger pores. First, the “permeability” of a cylindrical pore is proportional to the square of the pore radius  $R$ , whereas the capillary driving force is inversely proportional to  $R$ . Hence, even if capillary forces are smaller in bigger pores the velocity is still larger due to the higher permeability. The other reason is that the pores that were originally filled with oil will maintain an oil film at the wall, which is only slowly removed. In other words, a water-wet medium will effectively be oil-wet in the early stages of imbibition. The slow removal rate of an oil film shows itself in experiments on contact angle measurements. For water-wet media with a finite contact angle, it is possible that the delay time is a few months. This effect is observed in many spontaneous imbibition experiments (Topp et al. 1967; Smiles et al. 1971; Vachaud et al. 1972; Elzefrawy and Mansell 1975; Stauffer 1978; Tang and Firoozabadi 2001; Siemons et al. 2006; Plug and Bruining 2007; Plug et al. 2008; Yu et al. 2009). During the transition, the wetting fluid relative permeability is higher than in steady state conditions. Similarly, during the redistribution of the flow paths both the relative permeability of the non-wetting fluid and the capillary pressure are lower than in steady-state flow. Strictly speaking, this reasoning implies that the relative permeability and capillary pressure functions obtained in steady-state flow experiments cannot be used in transient processes whose characteristic transition times are comparable with characteristic fluid redistribution times. However, due to the monotonous

behavior of these functions, (see **Fig. 4**), they can still be used to characterize transient flow by evaluating the functions at some effective water saturations. Indeed, the relative permeabilities and the capillary pressure are evaluated not at the actual instantaneous values of the saturation  $S_w$ , but at some effective saturation  $\eta \geq S_w$ , see Fig. 4. The effective saturation  $\eta$  is always larger than the water saturation  $S_w$  or equal to it when steady state is attained. The concept of effective saturation was first introduced by Barenblatt and his colleagues (Barenblatt 1971; Barenblatt and Gilman 1987; Barenblatt et al. 1997, 2003). It is equivalent to an alternative formulation introduced by Hassanizadeh and Gray (1993) (see also Hassanizadeh et al. 2002).

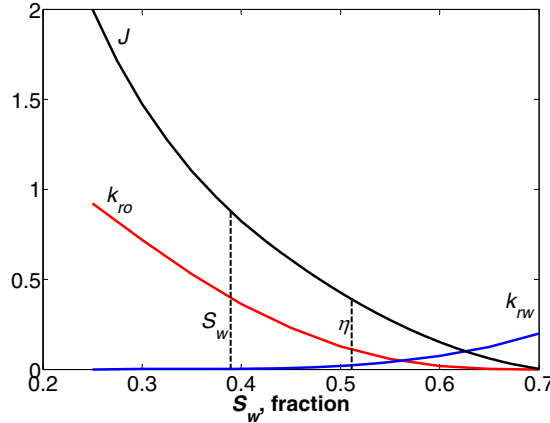


**Fig. 4—The effective saturation  $\eta$  (Eq. 10) is always higher than the actual water saturation  $S_w$ .**

In general, the effective saturation  $\eta$  can be different for both the relative permeability curves ( $k_{ra}$ ) and the Leveret  $J$ -function ( $J$ ). However, following Barenblatt (1971), Barenblatt and Gilman (1987), and Barenblatt et al. (2003), we assume that the effective saturation is the same for all three functions. Thus, instead of the relationships in Eq. 8 we have

$$k_{rw} = k_{rw}(\eta), \quad k_{ro} = k_{ro}(\eta), \quad P_c(\eta) = \sigma_{wo} \sqrt{\frac{\phi}{k}} J(\eta), \quad (9)$$

where the functions  $k_{rw}$ ,  $k_{ro}$ , and  $J$  are the same functions as in Eq. 8.

Due to the non-equilibrium effects, the relationship between  $\eta$  and  $S_w$  must be a time-dependent function. We use the hypothesis (Barenblatt 1971; Barenblatt et al. 1997, 2003) that there is a relationship between the local effective water saturation  $\eta$  and the actual water saturation  $S_w$  and its rate of change  $\partial S_w / \partial t$ . Dimensional analysis suggests that such a relationship must include a characteristic redistribution time. Further, linearization of this relationship yields

$$\tau_b \frac{\partial S_w}{\partial t} = \eta - S_w. \quad (10)$$

Here,  $\tau$  is a coefficient having the dimension of time. If the effective water saturation  $\eta$  were fixed and  $\tau$  were constant, then the difference  $(\eta - S)$  would decay exponentially as  $\exp(-t/\tau)$ . Therefore,  $\tau$  is a characteristic relaxation time (delay time) needed for the rearrangement of the menisci and flow paths to a new steady state configuration. Note that in spontaneous imbibition such a steady state is never achieved. Indeed, the redistribution time,  $\tau$ , may depend on the saturation, but we assume that  $\tau$  is constant.

### Upscaled Model

The previously derived upscaled equations (Salimi and Bruining 2010b) in the VFR with homogenization are

$$\frac{\partial}{\partial t} (\varphi_f S_{wf}) - \nabla_b \cdot (\lambda_{wf} \nabla_b \Phi_{wf}) + \frac{1}{|\Omega|} \int_{\Omega_m} \left\{ \frac{\partial}{\partial t} (\varphi_m S_{wm}) - \frac{\partial}{\partial z} \left( \lambda_{wm} \frac{\partial}{\partial z} \Phi_{wm} \right) \right\} d\mathbf{x}_s = q_{ext,w} \quad \text{in } Q, \quad (11)$$

$$-\nabla_b \cdot \left( (\lambda_{wf} + \lambda_{of}) \nabla_b \Phi_{wf} + \lambda_{of} \nabla_b \Phi_{cf} \right) + \frac{1}{|\Omega|} \int_{\Omega_m} \left\{ -\frac{\partial}{\partial z} \left( (\lambda_{wm} + \lambda_{om}) \frac{\partial}{\partial z} \Phi_{wm} + \lambda_{om} \frac{\partial}{\partial z} \Phi_{cm} \right) \right\} d\mathbf{x}_s = q_{ext,w} + q_{ext,o} \quad \text{in } Q, \quad (12)$$

where  $q_{ext,w}$  and  $q_{ext,o}$  are the external flow rates that come from the production and injection wells. The phase potential  $\Phi_\alpha$  is equal to the pressure ( $P$ ) plus the gravity term. Here, we also define the capillary potential  $\Phi_c = P_c + (\rho_o - \rho_w)gz$ . The integral term is the exchange term of fluid flow at the interface between the fracture and matrix. Here, the global fracture porosity and (effective) permeability are given as

$$\varphi_f = \frac{1}{|\Omega|} \int_{\Omega_f} \varphi_f^* d\mathbf{x}_s, \quad (13)$$

$$k_f = \frac{1}{|\Omega|} \int_{\Omega_f} k_f^* (\mathbf{I} + \nabla_s \otimes (\omega_1, \omega_2, 0)) d\mathbf{x}_s. \quad (14)$$

We use  $\phi_f^*$  to denote the intrinsic fracture porosity, and  $|\Omega|$  to denote the combined fracture and matrix domain. The integration is over the local domain, which is a small unit cell that contains a specific matrix-column size and fracture aperture for the grid cell. In the same way, we use  $k_f^*$  to denote the intrinsic fracture permeability. The behavior of  $\omega_1$  ( $\omega_2$ ) is a measure of the potential fluctuation caused by the non-homogeneous nature of the fractured reservoir that is subjected to a global potential gradient in the  $x$ -direction ( $y$ -direction). The VFR does not need an upscaling procedure in the  $z$ -direction, which is a reason that we only consider the vector  $(\omega_1, \omega_2, 0)$ . The cell equation required to solve for  $(\omega_1, \omega_2, 0)$  can be found in Salimi and Bruining (2010b).

To include the non-equilibrium effects in the upscaled model, we couple Eqs. 9 and 10 for Barenblatt's approach to the matrix-column equations. The equations for the matrix columns using Barenblatt's approach are

$$\frac{\partial}{\partial t} (\phi_m S_{wm}) - \nabla_s \cdot (\lambda_{wm}(\eta) \nabla_s \Phi_{wm}) = 0 \quad \text{in } B_m, \quad (15)$$

$$-\nabla_s \cdot ((\lambda_{wm}(\eta) + \lambda_{om}(\eta)) \nabla_s \Phi_{wm} + \lambda_{om} \nabla_s \Phi_{cm}(\eta)) = 0 \quad \text{in } B_m, \quad (16)$$

and Eq. 10. At the interface between the fracture and matrix systems, there are continuity of water and oil flow and continuity of capillary pressure. The boundary conditions on the vertical faces of the matrix columns read

$$\Phi_{wm}(t, x_b, x_s) = \Phi_{wf}(t, x_b), \quad \text{and} \quad \Phi_{cm}(t, x_b, x_s, \eta) = \Phi_{cf}(t, x_b), \quad (17)$$

where  $x_b$  denotes the global scale and  $x_s$  denotes the local scale. Our choice for the small-unit scale is a single matrix column of which vertical faces are surrounded by fractures and its horizontal faces (e.g., top and bottom) are connected to the cap and base rock. We define the global scale as the dimension of the grid-block scale.

There are no-flow boundary conditions on the top and bottom of the entire fractured reservoir, i.e.,

$$-\lambda_{\alpha\zeta} \nabla \Phi_{\alpha\zeta} \cdot \mathbf{n} = 0, \quad \alpha = w, o, \quad \text{and} \quad \zeta = f, m, \quad (18)$$

where  $\mathbf{n}$  denotes the outward unit normal vector to the surface.

The derivation of the upscaled model including the non-equilibrium effects is complete. To our knowledge, there exist no analytical nor numerical results for the upscaled-VFR model described above. In Appendix A, we develop an efficient numerical method to solve the complex system of upscaled equations for a vertically fractured reservoir.

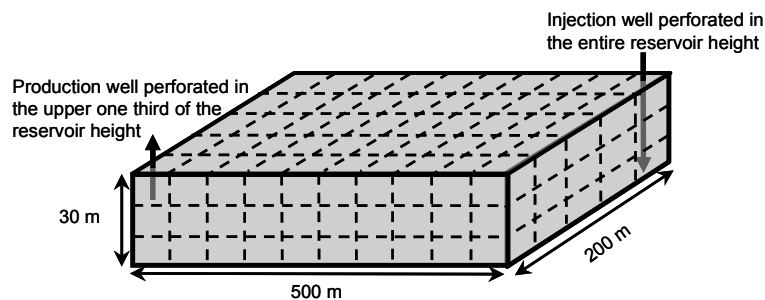


Fig. 5—Fractured reservoir waterflooding pattern.

## Results and Discussion

In this Section, we present the results of the numerical simulation. It is important to note that all our results are only valid for truly fractured reservoirs, i.e., reservoirs for which the fracture permeability is one order of magnitude larger (with respect to the scaling ratio) than the matrix permeability. We consider a vertically fractured oil reservoir with a length of 500 m, width of 200 m, and height of 30 m. Initially, the reservoir is saturated with oil. The initial water saturation both in the fracture and in the matrix is equal to the irreducible water saturations ( $S_{w,ir}$ ). As shown in Fig. 5, water is injected through the entire height of the reservoir from one corner and subsequently oil and water are produced through the upper third of the reservoir height at the diagonally opposite corner. Table 1 shows the basic input data for the numerical simulations. For each simulation case, the water injection rate is uniform. Table 2 shows the calculated effective (global) fracture permeabilities based on the different values of the lateral matrix-column size. Because fracture and matrix are considered as two different media, we use two different capillary-pressure and relative-permeability curves. Fig. 6 shows the capillary-pressure curves for the base case, i.e., contact angle of zero and completely water-wet. Fig. 7 shows the relative-permeability curves both for the fracture and for the matrix. We discretize the fractured reservoir into  $10 \times 5 \times 9$  grid cells in the  $x$ -,  $y$ -, and  $z$ -direction. Hence, there are 450 grid cells for the fracture system, which contains  $10 \times 5$  columns. Each column, which extends from the base rock to the cap rock, is

subdivided in a stack of nine matrix blocks. In other words, corresponding to each fracture grid cell on the base plane, there is a single matrix column, consisting of a stack of nine matrix blocks. We use  $9 \times 9 \times 9$  grid cells in the  $x$ -,  $y$ -, and  $z$ -direction for each representative matrix column. Therefore, we have a total of  $10 \times 5 \times 9$  grid cells for the fracture part and  $(10 \times 5 \times 9) \times 9 \times 9$  grid cells to represent the matrix part leading to a total of 36900 grid blocks.

Initial reservoir pressure (MPa)	27.5	Oil viscosity, $\mu_o$ (cp)	2
Bottomhole pressure in production wells (MPa)	26.9	Oil density, $\rho_o$ (kg/m <sup>3</sup> )	833
Well radius (m)	0.1524	Water viscosity, $\mu_w$ (cp)	0.5
Fracture aperture, $\delta$ ( $\mu\text{m}$ )	100	Water density, $\rho_w$ (kg/m <sup>3</sup> )	1025
Local fracture porosity, $\phi_f^*$	1	Residual oil saturation in matrix, $S_{or,m}$	0.3
Intrinsic fracture permeability, $k_f^*$ (D)	844	Residual oil saturation in fracture, $S_{or,f}$	0
Matrix porosity, $\phi_m$	0.19	Irreducible water saturation in matrix, $S_{w,ir,m}$	0.25
Matrix permeability, $k_m^*$ (mD)	1	Irreducible water saturation in fracture, $S_{w,ir,f}$	0

Lateral Matrix-Column Size, $\ell$ (m)	Global Fracture Permeability in the $x$ - and $y$ -direction, $k_{f,xy}$ (mD)	Global Fracture Permeability in the $z$ -direction, $k_{f,z}$ (mD)	Global fracture porosity, $\phi_f$
0.5	169	338	$4 \times 10^{-4}$
2	42	84	$1 \times 10^{-4}$
4	21	42	$5 \times 10^{-5}$

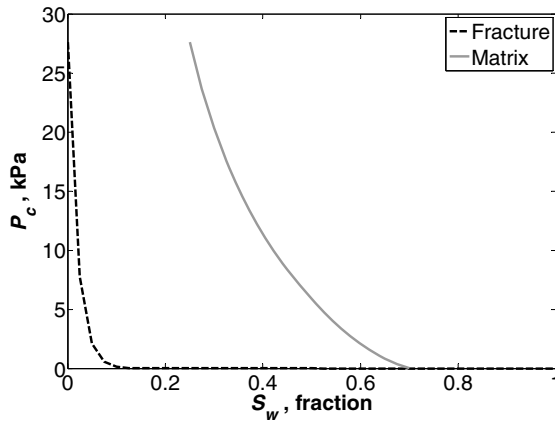


Fig. 6—Capillary-pressure curves versus water saturation.

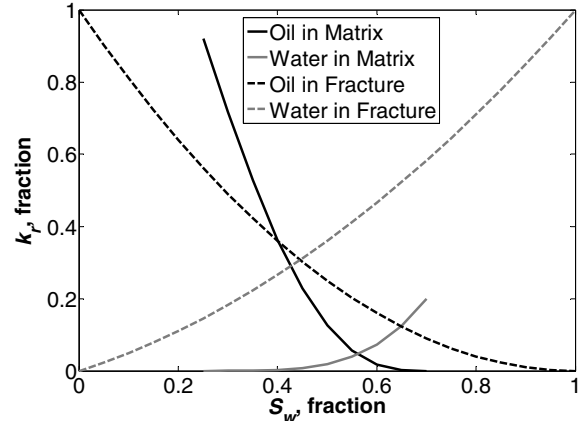


Fig. 7—Relative-permeability curves versus water saturation.

We characterize the behavior of a VFR by considering the three most important dimensionless numbers. These dimensionless numbers are previously discussed in Salimi and Bruining (2010b, 2010c), but for reasons of easy reference we briefly include the definition also in this paper. First, we define the Peclet number as the ratio of the capillary-diffusion time in the matrix columns and the residence time of the water in the fracture system. This Peclet number can be expressed as

$$\text{Pe} = \frac{\ell^2 u_{fw}}{D_{cap} L}, \quad \text{where} \quad D_{cap} = -\frac{\lambda_o \lambda_w}{\lambda_o + \lambda_w} \frac{dP_c}{dS_w}. \quad (19)$$

Here,  $\ell$  is the lateral matrix-column size,  $u_{fw}$  is the water injection rate,  $\lambda_\alpha$  is the mobility of phase  $\alpha$  (oil, water), and  $L$  is the distance between wells. The capillary-diffusion coefficient  $D_{cap}$  is evaluated in the matrix domain. In Eq. 19, the capillary-diffusion coefficient is a strongly nonlinear function of the water saturation. Consequently, its values change with time and space. As mentioned above, the initial water saturation both in the fracture and in the matrix is equal to the connate water saturations ( $S_{wc}$ ). Consequently, the capillary-diffusion coefficient ( $D_{cap}$  in Eq. 19) is initially zero for both the fracture and matrix, and remains zero at an early injection time for those regions that are far from the injection well. Therefore, if we use the geometric mean and/or harmonic mean, the average capillary-diffusion coefficient would become zero and/or infinity, respectively. However, for average over time, there is not such a problem. In addition, the geometric mean is a type of mean or average, which indicates the central tendency or typical value of a set of numbers, whereas the arithmetic mean is not a robust statistic, meaning that it is greatly influenced by outliers. This is the case for higher injection rates because the water slightly penetrates to the matrix over long time of the simulation. Therefore, we use an arithmetic mean over the space and a geometric

mean over time to obtain a single averaged value of the Peclet number for each case discussed below. The second dimensionless number is the gravity number that expresses gravity forces over viscous forces in the fracture system. We use the following expression for this gravity number (Yortsos 1991; Shook et al. 1992)

$$N_G = \frac{k_f \Delta \rho g H}{\mu_w u_{fw} L}, \quad (20)$$

where  $H$  is the height of the reservoir,  $k_f$  is the effective (global) fracture permeability,  $u_{fw}$  is the global water injection rate, and  $\Delta \rho$  is the density difference between water and oil phase.

In the simulations, we vary the contact angle, capillary-pressure curve (mixed-wet), and delay time (characteristic relaxation time),  $\tau$ , to investigate the effect of wettability on the performance of waterdrive recovery from VFRs for different water injection rates and lateral matrix-column sizes. In all cases, the cumulative oil production is the basis for the comparison. Note that we express the (dimensionless) time in terms of cumulative pore volume (PV) water injected.

**Fig. 8** shows the oil saturation history after water injection in the two NE corner columns, with production in the top 1/3 of the two SW corner columns. The water saturation first expands via the bottom of the reservoir. We observe in Fig. 8 that co-current (gravity) and counter-current imbibition occur at the same time.

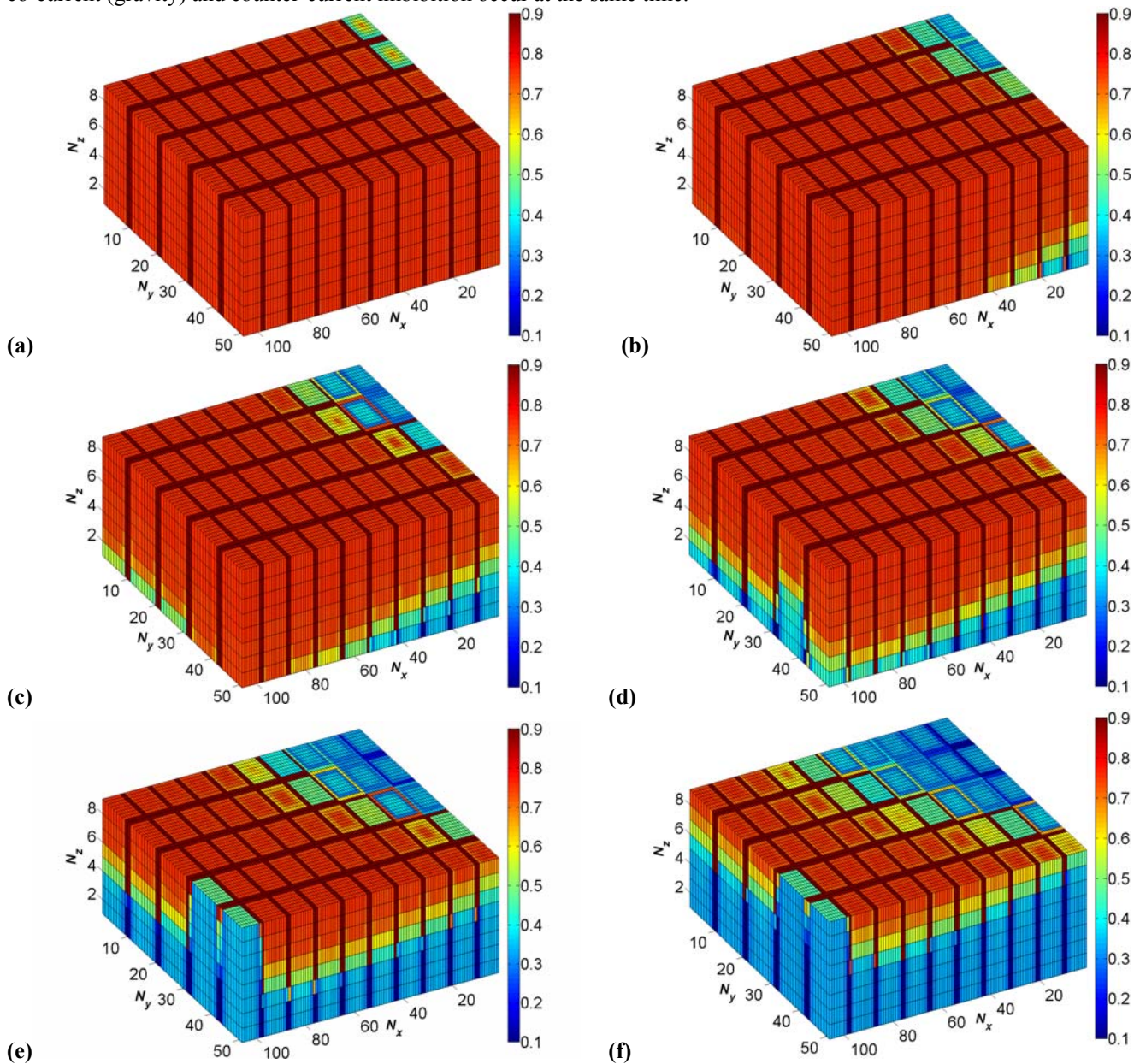


**Fig. 8**—Oil Saturation history at (a)  $t = 50$  days, (b)  $t = 375$  days, (c)  $t = 625$  days, (d)  $t = 750$  days, (e)  $t = 1250$  days, and (f)  $t = 2000$  days. The reservoir has a length of 500 m in the  $x$ -direction, 200 m in the  $y$ -direction and 30 m in the  $z$ -direction. The water injection rate is 0.1 PV/yr and the lateral matrix-column size is 0.5 m. First, the water occupies the bottom of the reservoir. Then, the water rises in the fractures and finally the water rises in the columns. Due to gravity, the oil at the top of the reservoir is not fully depleted.

### Effect of Contact Angle

**Fig. 9a** shows the effect of contact angle on the cumulative oil production for a water injection rate of  $q_w = 0.1$  PV/yr and a lateral matrix-column size of  $\ell = 0.5$  m. From  $t = 0$  to 0.06-0.24 PV depending on the contact angle, the ratio of water production/water injection is small  $\approx 0.03$ , but non-zero due to the small fracture porosity. At  $t = 0.06$  PV, significant water production occurs for  $\theta = 80^\circ$  and at  $t = 0.24$  PV for  $\theta = 0^\circ$ . Trivially, the cumulative-production curves before the first significant water breakthrough are identical. The recovery ratio of the cumulative oil production at  $\theta > 0^\circ$  and  $\theta = 0^\circ$  is denoted by  $\Xi$ . We use this ratio as an indicator for comparison. After breakthrough occurs for  $\theta = 80^\circ$ , the recovery ratio decreases and reaches its minimum value of 0.74 at the time that water breaks through for  $\theta = 0^\circ$  ( $t = 0.24$  PV). After that, the recovery ratio increases and reaches 0.94 at  $t = 1.83$  PV. The same trend is also observed for other contact angles in comparison to  $\theta = 0^\circ$ . **Fig. 9a** shows that the effect of contact angle below  $45^\circ$  is almost negligible.

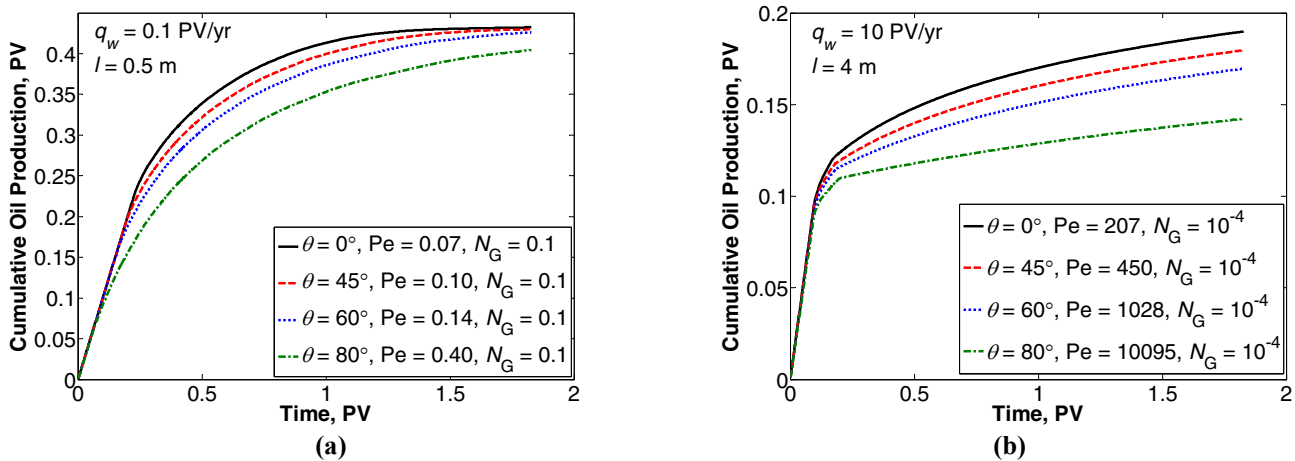


**Fig. 9**—Effect of contact angles on the cumulative oil production for (a) water injection rate of  $q_w = 0.1$  PV/yr and lateral matrix-column size of  $\ell = 0.5$  m, and (b) water injection rate of  $q_w = 10$  PV/yr and lateral matrix-column size of  $\ell = 4$  m.

The non-linear capillary-diffusion coefficient (see Eqs. 6 and 19) is proportional to the cosine of the contact angle, and we may expect a similar dependence for the oil recovery. However, due to complex interaction between various factors like continuity of capillary pressure at the interface between fracture and matrix, supply of water via the fractures, and gravity effects, the production rates are not proportional to  $\cos \theta$ ; however, they are indeed slower for higher contact angles. The reason for this is that initially the capillary-diffusion rate is inversely proportional to the square root of time and therefore extremely fast. Hence, the amount of water initially absorbed by the matrix columns and consequently the oil expelled from the matrix columns is determined by the water supply rate irrespective of the contact angle. For the low values of the Peclet number ( $0.1 < Pe < 0.4$ ) used in the results of **Fig. 9a**, the residence time of water in the fracture is long. This means that all the matrix columns in contact with water will expel their oil into the fractures. However, low water injection rates (i.e.,  $q_w = 0.1$  PV/yr) lead to relatively high gravity numbers ( $N_G = 0.1$ ) and therefore gravity segregation occurs, keeping water away from the top part of the reservoir. As a result, regions not in contact with water will not produce oil. Gravity segregation will be more pronounced at high contact angles, because then the mixing tendency by capillary forces is reduced. In the absence of gravity, the relative discrepancy between oil recoveries of different contact angles should be small for low Peclet numbers, because now the water can reach all parts of the reservoir. For this reason, we observe in **Fig. 9a** that after the effect of gravity disappears, the cumulative oil production for different contact angles lead to almost the same value.

**Fig. 9b** presents the effect of contact angle on the cumulative oil production for a high water injection rate of  $q_w = 10$  PV/yr and a lateral matrix-column size of  $\ell = 4$  m. In this case, the gravity number ( $N_G = 10^{-4}$ ) is low due to a high water injection rate. Therefore, significant water breakthrough occurs at almost the same time, i.e.,  $t = 0.1$  PV, for different contact angles. After that, the oil recovery ratio between oil recovery for  $\theta = 80^\circ$  and for  $\theta = 0^\circ$  decreases monotonically as time proceeds and reaches its minimum value of 0.75 at  $t = 1.8$  PV. Initially, capillary-diffusion rates are fast and the first oil produced comes partially from the fractures and partially from the outer boundaries of the matrix columns. After water breakthrough, capillary imbibition determines the rate of oil production due to the high value of the Peclet number ( $200 < Pe < 10^4$ ). The production after water breakthrough is more or less proportional to  $\cos \theta$ . As a result, the effect of contact angle on oil recovery for larger Peclet numbers (see **Fig. 9b**) is more pronounced, as expected.

**Figs. 10a and 10b** display the oil saturation profiles for a water injection rate of  $q_w = 0.1$  PV/yr with  $\theta = 0^\circ$  and  $\theta = 80^\circ$  at  $t = 500$  days, respectively. **Figs. 10a and 10b** reveal that at  $t = 500$  days, water breakthrough occurs for  $\theta = 80^\circ$  (**Fig. 10b**), but for  $\theta = 0^\circ$ , the water front is still far away from the production well (**Fig. 10a**). Water coning near the production well occurs as only the top third part of the well is open to the reservoir (see, however, **Fig. 5**). At later times (not shown here), water breakthrough occurs also for the  $\theta = 0^\circ$  case. For low water injection rates ( $q_w = 0.1$  PV/yr) and thus relatively high gravity numbers ( $N_G = 0.1$ ), the water is slumping underneath and except near the wells, the top part of the matrix columns will not initially be in contact with water, even if there is water breakthrough.

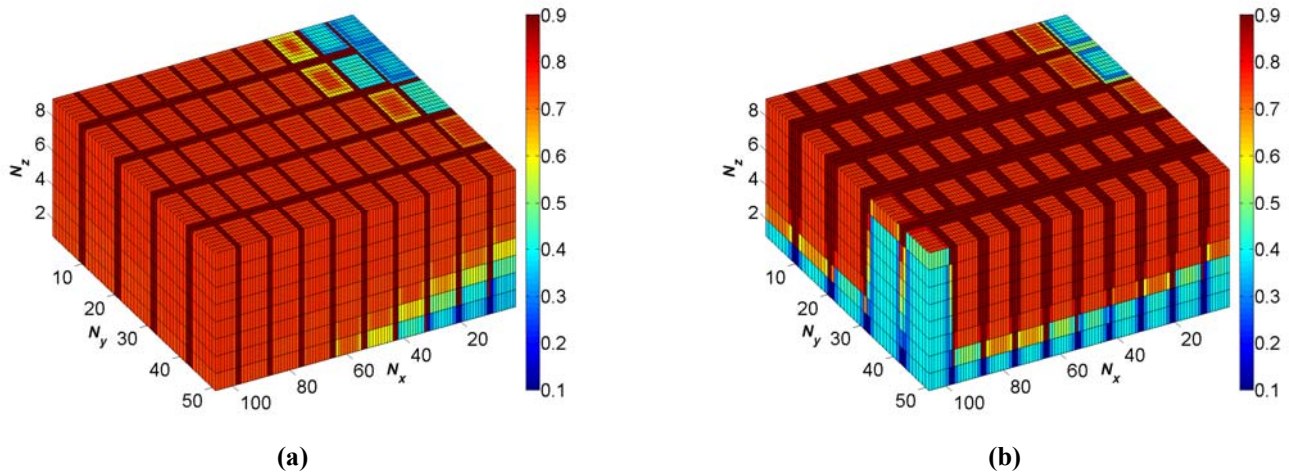


Fig. 10—Oil saturation profiles for a water injection rate of  $q_w = 0.1$  PV/yr and a lateral matrix-column size of  $\ell = 0.5$  m at  $t = 500$  days for (a)  $\theta = 0^\circ$  and (b)  $\theta = 80^\circ$ .

### Effect of mixed wetting

Here, we investigate the effect of mixed wetting on oil recovery for different water injection rates and lateral matrix-column sizes and compare to completely water-wet results. We consider three different wetting cases, viz., a water-wet fracture/mixed-wet matrix, a mixed-wet fracture/mixed-wet matrix, an oil-wet fracture/oil-wet matrix case. For the water-wet fracture/mixed-wet matrix case (i.e.,  $I_{w,f} = 1$ ,  $I_{w,m} = 0.5$ ), we use the capillary pressure functions shown in Fig. 3. **Figs. 11 and 12** display the capillary pressure functions for the mixed-wet fracture/mixed-wet matrix case (i.e.,  $I_{w,f} = I_{w,m} = 0.5$ ) and for the oil-wet fracture/oil-wet matrix case (i.e.,  $I_{w,f} = I_{w,m} = 0$ ), respectively.

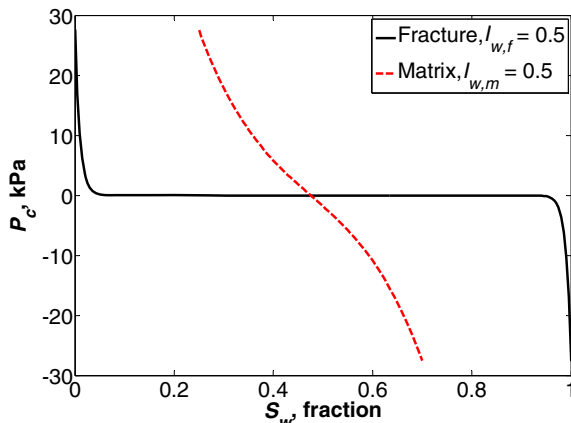


Fig. 11—Capillary-pressure curves for mixed-wet fracture/mixed-wet matrix.

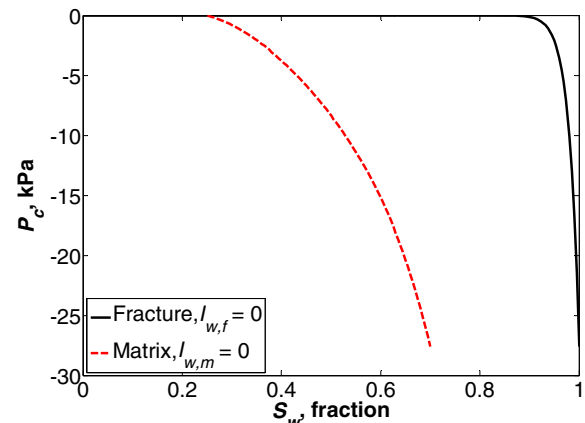


Fig. 12—Capillary-pressure curves for oil-wet fracture/oil-wet matrix.

In a (strongly) water-wet reservoir (i.e.,  $I_{w,f} = I_{w,m} = 1$ ), the displacement of oil from the matrix will often be dominated by capillary forces, and hence be called water/oil imbibition. Two different imbibition regimes that can be considered are counter-current and co-current imbibition. In the co-current imbibition process, the oil/water capillary transition zone is moving inside the matrix ahead of the oil/water contact in the fracture system. In this case, oil will leave the matrix blocks near the top of the blocks and water will enter the matrix blocks from the bottom. Counter-current imbibition occurs when the fracture oil/water contact is rising very quickly, e.g., in the case of high injection rates and/or of a very sparse fracture network, whereas co-current (gravity) imbibition will prevail with a relatively slower rise of the oil/water contact zone in the fracture.

In a strongly oil-wet reservoir ( $I_{w,f} = I_{w,m} = 0$ ), oil can be displaced from the matrix by water only by gravity forces, with capillary forces trying to retain the oil. In such a case, the water/oil gravity drainage process is taking place below the fracture oil/water contact.

In a reservoir that is not strongly oil-wet nor water-wet, but of some intermediate wettability ( $0 < I_{w,f}, I_{w,m} < 1$ ), the recovery process in the water-invaded part of the reservoir is a combination of water/oil gravity drainage and water/oil capillary imbibition.

**Fig. 13a** shows the effect of mixed wetting on oil production for a water injection rate of  $q_w = 0.1$  PV/yr and a lateral matrix-column size of  $\ell = 0.5$  m. In the case of mixed wetting, part of the pore space is oil-wet and hence will not be invaded by water. This effect can clearly be observed from Fig. 13a, where the cumulative oil production for the water-wet fracture/mixed-wet matrix case ( $I_{w,f} = 1$ ,  $I_{w,m} = 0.5$ ), reaches a maximum value at  $t = 0.35$  PV as indicated by the horizontal

cumulative-production curve. The characteristic ( $\bar{\mathcal{E}}$ ) is for the mixed-wet case the ratio of the cumulative production of the not completely water-wet case divided by the cumulative production of the completely water-wet case ( $I_{w,f} = I_{w,m} = 1$ ). Values of  $\bar{\mathcal{E}}$  can be inferred from the Figures. The characteristic ratio  $\bar{\mathcal{E}}$  for three cases is initially equal to one. Subsequently, when water breakthrough occurs for the water-wet fracture/mixed-wet matrix case ( $t = 0.1$  PV), it monotonically decreases until it reaches a minimum value of  $\bar{\mathcal{E}} = 0.52$  at  $t = 1.8$  PV. Indeed, for low Peclet numbers ( $Pe \approx 0.07$ ), the ultimate oil recovery is reached at  $t = 0.35$  PV for  $I_{w,f} = 1$ ,  $I_{w,m} = 0.5$  and is about half the recovery obtained for completely water-wet reservoirs. The final recovery ratio ( $\bar{\mathcal{E}} = 0.52$ ) for this case, is about equal to the Amott index ( $I_{w,m} = 0.5$ , see Eq. 7). This behavior is in contrast with the behavior observed in Fig. 8a for high contact angles ( $\theta = 80^\circ$ ), where eventually all mobile oil from the matrix columns is produced. All the same, the recovery for the water-wet fracture/mixed-wet matrix case is much less than for the finite contact angle water-wet case.

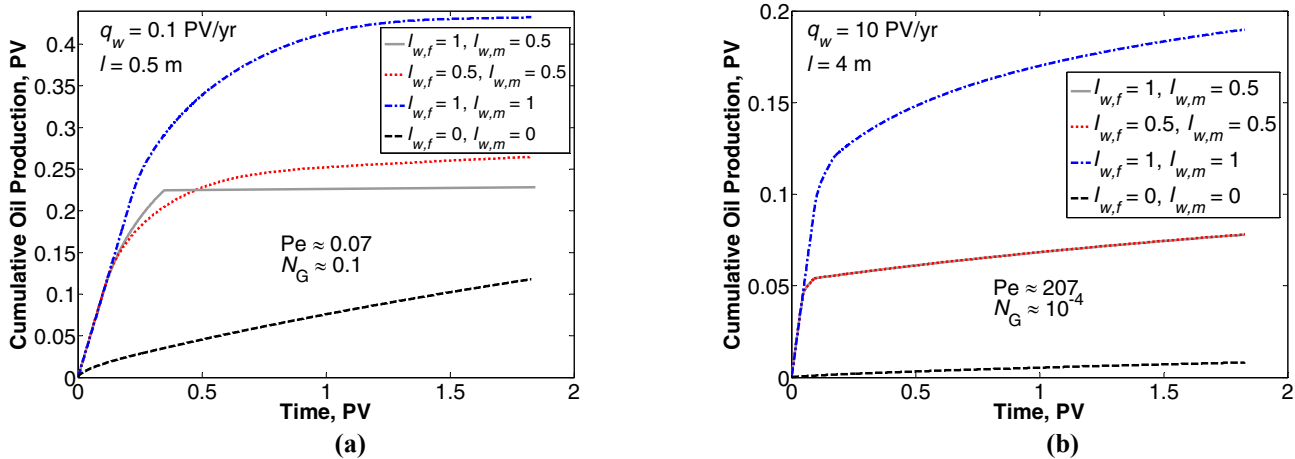


**Fig. 13—Effect of mixed wetting on the cumulative oil production for (a) water injection rate of  $q_w = 0.1$  PV/yr and lateral matrix-column size of  $l = 0.5$  m, and (b) water injection rate of  $q_w = 10$  PV/yr and lateral matrix-column size of  $l = 4$  m.**

For the mixed-wet fracture/mixed-wet matrix case ( $I_{w,f} = 0.5$ ,  $I_{w,m} = 0.5$ ), the recovery ratio  $\bar{\mathcal{E}}$  monotonically decreases until a minimum value of  $\bar{\mathcal{E}} = 0.6$  is reached at  $t = 1.3$  PV. After that, it starts increasing as the fracture system is almost entirely filled with water and oil/water gravity drainage starts contributing to oil production. The characteristic ratio becomes  $(I_{w,f} = 0.5, I_{w,m} = 0.5)/(I_{w,f} = 1, I_{w,m} = 0.5) = 0.62$  at  $t = 1.8$  PV as shown in Fig. 13a. In the long time (not shown here), all mobile oil should be produced for this case. This behavior is contrary to the behavior of the water-wet fracture/mixed-wet matrix case. The reason is that, indeed, for  $I_{w,f} = 0.5$ ,  $I_{w,m} = 0.5$ , the recovery process is a combination of water/oil gravity imbibition and water/oil capillary imbibition, whereas for  $I_{w,f} = 1$ ,  $I_{w,m} = 0.5$ , the only recovery process is oil/water capillary imbibition.

For the oil-wet fracture/oil-wet matrix case ( $I_{w,f} = 0.5$ ,  $I_{w,m} = 0.5$ ), the recovery ratio monotonically decreases and reaches its minimum value of  $\bar{\mathcal{E}} = 0.1$  at the time that water breaks through for the completely water-wet ( $t = 0.24$  PV). Afterward, because significant water breakthrough occurs for the completely water-wet, the recovery ratio increases and reaches 0.3 at  $t = 1.83$  PV. However, we observe from Fig. 13a that the cumulative oil production for the completely oil-wet system is low compared to the other cases. The main reason is that the only possible way to displace oil from the matrix columns is by gravity forces and because the gravity forces are not large enough the rate of oil/water gravity drainage is low.

**Fig. 13b** presents the effect of mixed wetting on the cumulative oil production for a high water injection rate of  $q_w = 10$  PV/yr and a lateral matrix-column size of  $l = 4$  m. We observe from Fig 13b that the cumulative oil production for  $I_{w,f} = 1$ ,  $I_{w,m} = 0.5$  is the same as  $I_{w,f} = 0.5$ ,  $I_{w,m} = 0.5$ . For these two cases, the recovery ratio starts decreasing at  $t = 0.04$  PV until a minimum value of  $\bar{\mathcal{E}} = 0.40$  is reached at  $t = 1$  PV. Then, it starts increasing as also substantial water breakthrough occurs for the completely water-wet case. The recovery ratio is  $\bar{\mathcal{E}} = 0.41$  at  $t = 1.83$  PV. However, the recovery ratio for the water-wet fracture/mixed-wet matrix case, achieves an asymptotic value that is equal to the matrix Amott index ( $I_{w,m} = 0.5$ ), whereas for the mixed-wet fracture/mixed-wet matrix case, the asymptotic value would be equal to the movable oil. Moreover, for high Peclet numbers ( $Pe \approx 207$ ), the ultimate oil recovery for  $I_{w,f} = 1$ ,  $I_{w,m} = 0.5$  is not yet reached at  $t = 2$  PV in contrast with low Peclet numbers (see Fig. 13a). For the completely oil-wet case, the recovery ratio reaches a minimum value of  $\bar{\mathcal{E}} = 0.01$  at  $t = 0.1$  PV when the cumulative-oil-production curve for completely water-wet starts to deviate considerably from the initial straight line. Subsequently, it gradually increases and reaches a value of  $\bar{\mathcal{E}} = 0.04$  at  $t = 1.8$  PV. Indeed, for strongly oil-wet fractured reservoirs, waterflooding is not an efficient recovery process.

Overall, the cumulative oil production for all cases in Fig. 13b is much lower than that shown in Fig. 13a because for high water injection rates and large lateral matrix-column sizes, the Peclet number is much larger than for low water injection rates and small lateral matrix-column sizes ( $Pe \approx 207$  in Fig. 13b vs.  $Pe \approx 0.07$  in Fig. 13a). In other words, when Peclet numbers are large, the convective transport is dominant over imbibition and hence the oil recovery mechanism is limited by the rate of imbibition. Furthermore, the residence time of water is much shorter than the characteristic time of imbibition. As a result, less

fluid-flow exchange occurs for the same amount of injected water in comparison to low Peclet numbers. Thus, if we were in the high-Peclet-number regime, the recovery for the same amount of injected water would be low accordingly.

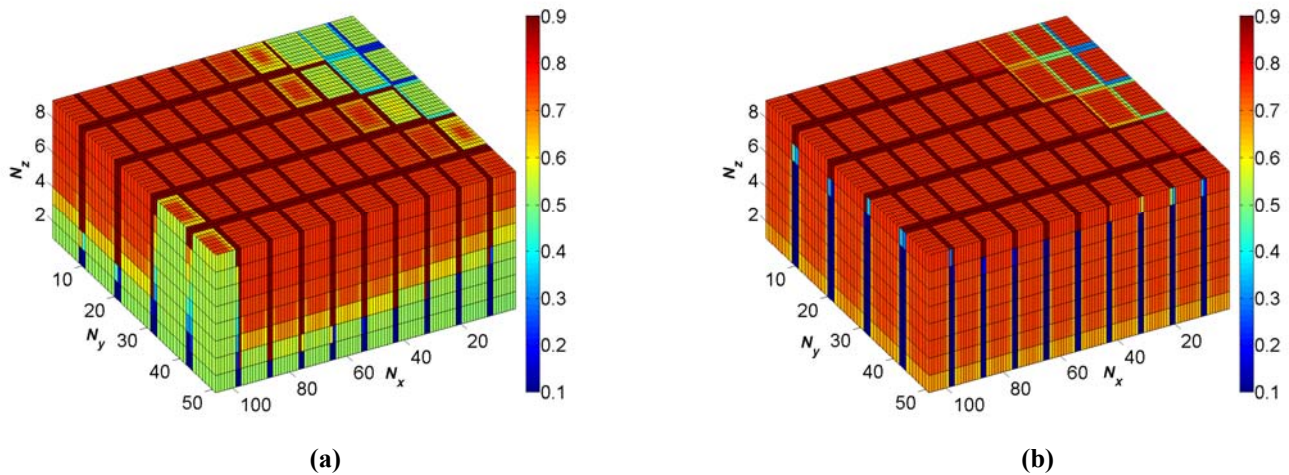


**Fig. 14—Oil saturation profiles for a water injection rate of  $q_w = 0.1$  PV/yr and a lateral matrix-column size of  $\ell = 0.5$  m at  $t = 500$  days for (a) mixed-wet fracture/mixed-wet matrix ( $I_{w,f} = I_{w,m} = 0.5$ ) and (b) oil-wet fracture/oil-wet matrix ( $I_{w,f} = I_{w,m} = 0$ ).**

**Figs. 14a and 14b** display the oil saturation profiles for a water injection rate of  $q_w = 0.1$  PV/yr for  $I_{w,f} = I_{w,m} = 0.5$  and  $I_{w,f} = I_{w,m} = 0$  at  $t = 500$  days, respectively. Figs. 14a reveals that at  $t = 500$  days, water breakthrough occurs and water is slumping underneath except near the wells. However, Fig. 14 b shows that water breakthrough also happens and the fractures are almost filled with the injected water and thus the oil/water gravity drainage takes place at the bottom of the reservoir, while capillary forces try to retain the oil. Moreover, Figs. 14a and 14b clearly illustrate that much less injected water penetrates into the matrix columns for the completely oil-wet case due to the fact that in  $I_{w,f} = I_{w,m} = 0$ , only gravity forces contribute to oil production, whereas in  $I_{w,f} = I_{w,m} = 0.5$ , a combination of water/oil gravity drainage and water/oil capillary imbibition occur in the water-invaded part of the reservoir.

From what explained above, we conclude that in general, the efficiency of waterflooding depends on the shape of the fracture and the matrix capillary pressure.

**Effect of the Non-Equilibrium**

The third mechanism that changes the capillary-pressure behavior is the non-equilibrium effect, explained above. In this theory, the time to reach equilibrium is denoted by  $\tau$ . For the non-equilibrium effects, the capillary pressure and relative permeability functions are the same functions as shown in Figs. 6 and 7 respectively, but they are now evaluated at the effective water saturation ( $\eta$ ) instead.

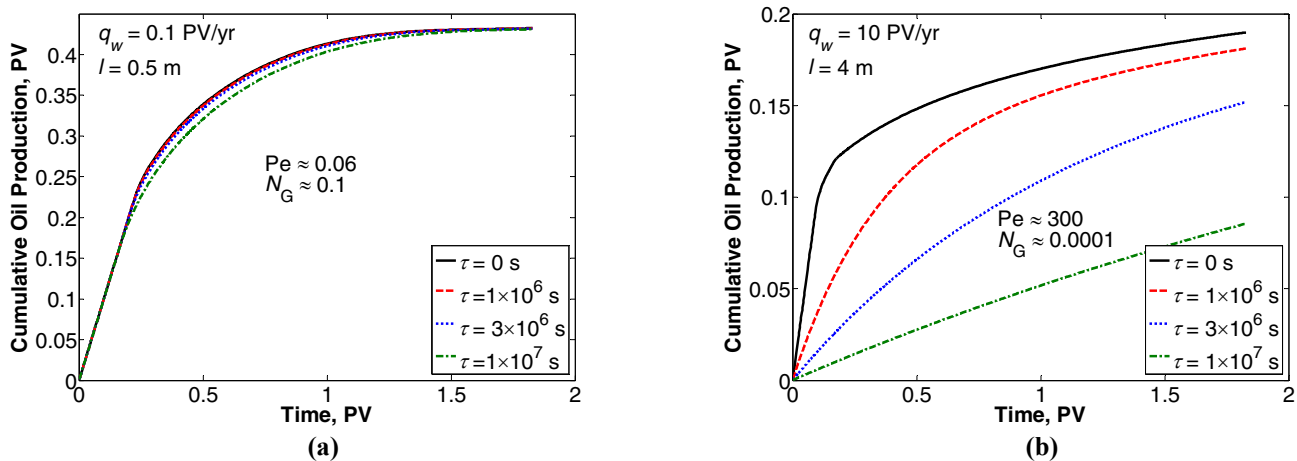


**Fig. 15—Effect of the delay time on the cumulative oil production for (a) water injection rate  $q_w = 0.1$  PV/yr and lateral matrix-column size of  $\ell = 0.5$  m, and (b) water injection rate of  $q_w = 10$  PV/yr and lateral matrix-column size of  $\ell = 4$  m.**

**Fig. 15a** shows the effect of the delay time on the cumulative oil production for a water injection rate of  $q_w = 0.1$  PV/yr and a lateral matrix-column size of  $\ell = 0.5$  m. Here, we define the oil recovery ratio between non-zero delay-time cases and the zero delay-time case. We observe from Fig. 15a that the delay time does not influence oil recovery substantially. The reason is that for low injection rates and thus low Peclet numbers (Fig. 15a,  $Pe \approx 0.06$ ), the residence time of water in the fracture (i.e., 0.25 PV or 913 days) is much longer than any reasonable delay time  $\tau$ . The residence time is the time at which the

cumulative-oil-production curve starts to deviate considerably from the initial straight line. In this case, the effect of the delay time is almost zero. On the other hand, we see from Fig. 15b that the delay time affects oil production significantly. Moreover, Fig. 15b reveals that significant water breakthrough immediately happens for non-zero delay-time cases. As a result, the recovery ratio starts decreasing from the beginning until it reaches its minimum value of 0.37, 0.16, and 0.06 respectively for  $\tau = 10^6$  sec,  $3 \times 10^6$  sec, and  $10^7$  sec at  $t = 0.1$  PV, the time at which water breakthrough occurs for  $\tau = 0$ . Subsequently, the recovery ratio increases and reaches a value of 0.95, 0.80, and 0.45 respectively for  $\tau = 10^6$  sec,  $3 \times 10^6$  sec, and  $10^7$  sec at  $t = 1.83$  PV. For high Peclet numbers ( $Pe \approx 300$ ), the residence time of water in the fractures is short, i.e., of the order of 0.1 PV or 3.65 days. In each of the non-zero delay-time cases shown in Fig. 15b, the delay time is much larger than the residence time and thus it influences the cumulative oil production considerably, as expected. In the laboratory, samples with long delay times are often erroneously considered oil-wet. This has consequences for any remediative action (Punternvold and Austad 2008; Punternvold et al. 2009) to enhance the imbibition rates.

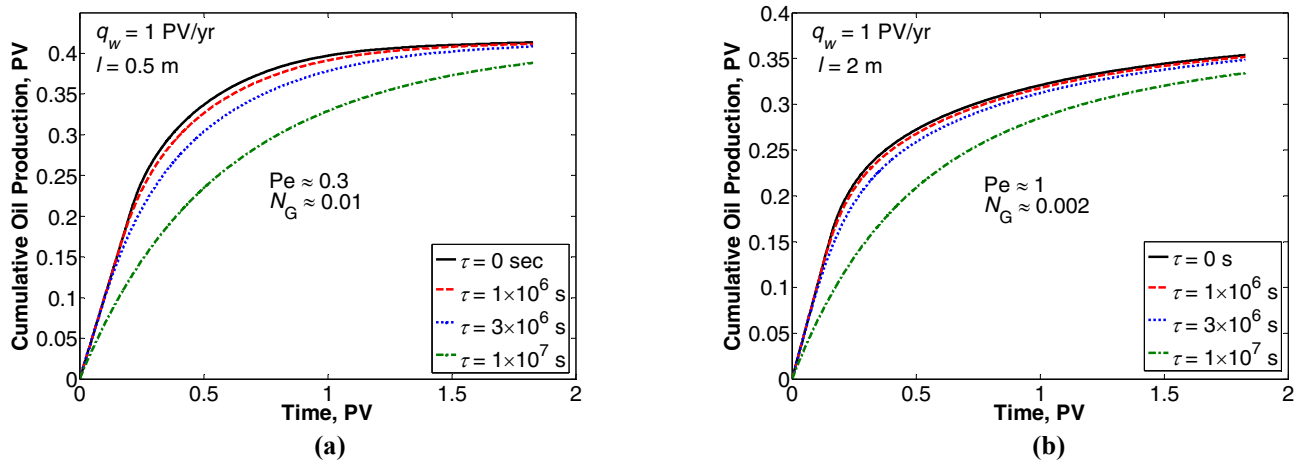


Fig. 16—Effect of the delay time on the cumulative oil production at a water injection rate  $q_w = 1$  PV/yr for (a) lateral matrix-column size of  $l = 0.5$  m and (b) lateral matrix-column size of  $l = 2$  m.

For intermediate Peclet numbers we distinguish two cases; one with small ( $l = 0.5$  m) and one with large ( $l = 2$  m) lateral matrix columns. Figs. 16a and 16b show the effect of the delay time on the cumulative oil production for a water injection rate of  $q_w = 1$  PV/yr and a lateral matrix-column size of  $l = 0.5$  m and  $l = 2$  m, respectively. The size of the matrix columns has an influence on the fracture spacing and hence the global fracture permeability (see Eq. 3). Therefore, this has also an effect on the gravity number (0.01 vs. 0.002). Moreover, the size of matrix-column size influences the Peclet number as well (0.3 vs. 1, see Eq. 19). We observe from Figs. 16a and 16b that the residence time of water is about 0.25 PV (90 days) and 0.18 PV (66 days), respectively. This is also reflected by the fact that the Peclet number for the  $l = 0.5$  m case ( $Pe \approx 0.3$ ) is smaller than for the  $l = 2$  m case ( $Pe \approx 1$ ). Figs. 16a and 16b reveal that the relative discrepancy for  $\tau = 10^6$  sec and  $3 \times 10^6$  sec is almost negligible, whereas for the longest delay time ( $10^7$  sec), there is an appreciable effect of the delay time, leading to a recovery ratio of only 0.59. For intermediate Peclet numbers, the residence time of the fluids and the delay time are of the same order of magnitude, meaning that for sufficiently long delay times ( $\tau = 10^7$  sec or 116 days), the behavior is completely different from the behavior of small delay times. As shown in Fig. 16a, the results for high gravity numbers show a somewhat larger dependence on the delay time than for small gravity numbers (Fig. 16b).

To emphasize the effect of the delay time on the displacement mechanism, we depict the oil saturation profiles in Figs. 17a and 17b for a water injection rate of  $q_w = 1$  PV/yr without delay time and with a delay time of  $\tau = 10^7$  sec at  $t = 50$  days, respectively. Fig 17a, for zero delay times, clearly illustrates that the water front is still far from the production well and water penetrates more into the matrix columns nearby the injection well, while Fig 17b with  $\tau = 10^7$  sec describes that water breakthrough has already occurred and hence less injected water imbibes in the matrix columns.

The general pattern observed in Figs. 15 and 16 also occurs for the non-equilibrium effects of Hassanizadeh's theory, the qualitative behavior is the same, and both approaches show the importance of taking into account the non-equilibrium effects in the capillary-pressure and relative permeability behavior. A full overview of similarities and differences between Barenblatt's and Hassanizadeh's approach for the non-equilibrium effects can be found in Salimi and Bruining (2010d).

The non-equilibrium effects have consequences for laboratory experiments. In the laboratory, a typical cylindrical core has a length of 20 cm and a diameter of 10 cm. In addition, a usual injection rate is 5 ml/min. To be able to calculate the Peclet number; we need to estimate the capillary-diffusion coefficient. We assume that the absolute permeability of the core is 1 mD. Moreover, we use the matrix relative permeability functions that are plotted in Fig. 7, and the average capillary derivative and the average mobility factor  $[\lambda_o \lambda_w / (\lambda_o + \lambda_w)]$  for calculating  $D_{cap}$ . Note that the characteristic length for the capillary diffusion and convection transport in a laboratory core is the same. Therefore, the definition for the Peclet number in Eq. 19 reduces to  $Pe_{lab} = U_{inj} L / D_{cap}$ . For the laboratory specifications mentioned above, the calculated Peclet number would be  $Pe_{lab} = 1768$ . Therefore, most of the laboratory experiments are in the high-Peclet-number regime. As a result, the non-equilibrium effects

have considerable effects on the rate of oil production. Consequently, in the laboratory, samples with long delay times and/or large capillary-damping coefficients are often erroneously considered oil-wet. This has consequences for any remediative action (Punternvold and Austad 2008; Punternvold et al. 2009) to enhance the imbibition rates.

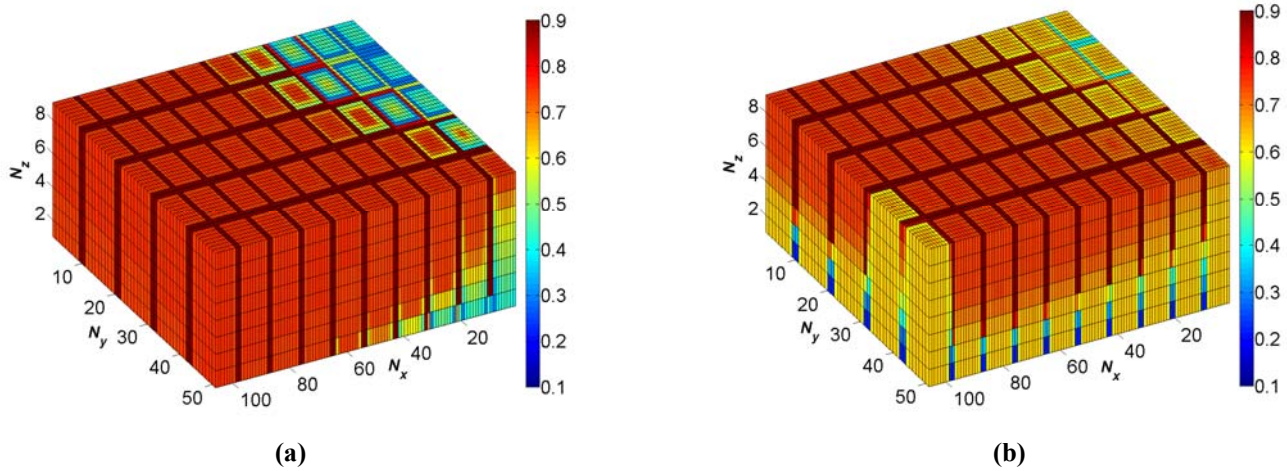


Fig. 17—Oil saturation profiles for a water injection rate of  $q_w = 1$  PV/yr and a lateral matrix-column size of  $\ell = 0.5$  m at  $t = 50$  days for delay times (a)  $\tau = 0$  sec and (b)  $\tau = 10^7$  sec.

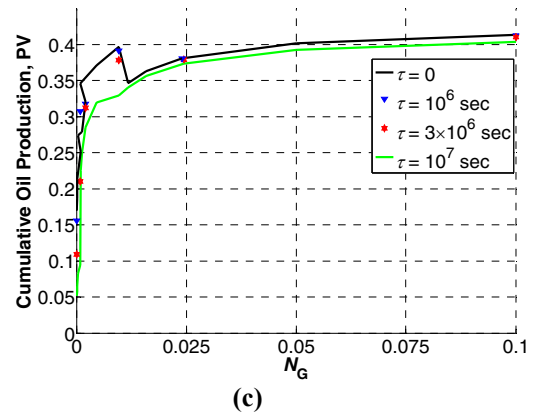
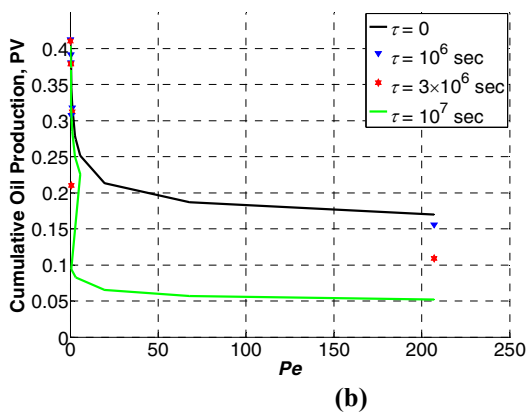
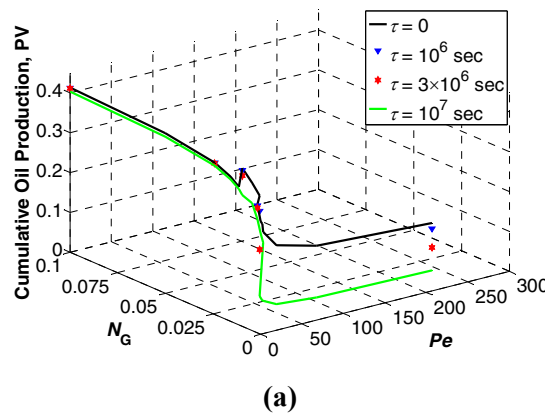


Fig. 18—Cumulative oil production at one PV injected water (a) versus the gravity number ( $N_G$ ) and the Peclet number ( $Pe$ ), (b) projected on the cumulative oil production-Peclet plane, (c) projected on the cumulative oil production-gravity number plane.

The salient features of the upscaled-VFR model including the non-equilibrium effects are summarized in Fig. 18, where the cumulative oil production at 1 PV is plotted versus the Peclet number ( $Pe$ ) and the gravity number ( $N_G$ ) for various delay times. At small gravity numbers and large Peclet numbers, the recovery is low. The recovery at small gravity numbers is rather insensitive to the Peclet number. As the gravity number increases and the Peclet number decreases, the recovery becomes much higher. It can be expected that here counter-current imbibition is replaced by the much more effective co-current gravity imbibition. Also, the rate of imbibition from the matrix column becomes larger compared to the rate of fluid transport in the fracture system. In the absence of delay times, the maximum recovery becomes higher than when delay times

are relevant. At a critical value of the gravity number-Peclet number, there is a sudden decrease in oil recovery when delay times are ignored. Therefore, there is a smooth transition between the two regimes, from small to large Peclet numbers. At high Peclet numbers, the rate of oil production becomes limited by imbibition from the matrix column and hence by the delay time. One may speculate that the transition where the result is independent of the imbibition rate, due to long residence times of fluids in the fracture, to the situation at large Peclet numbers where it does become sensitive to the imbibition rate is unstable. For this reason, in the absence of delay times, a peak of relative high oil recovery occurs.

## Conclusions

We derive a physically based upscaled model in which the non-equilibrium effect in capillary pressure and relative permeabilities is included for a vertically fractured reservoir (VFR) using homogenization. We also develop a computationally efficient numerical scheme to solve the upscaled-VFR model. The simulations show that the Peclet number plays a central role:

- At low Peclet numbers, the rate of imbibition dominates over the convective transport in the fracture. Therefore, the characteristic time of fluid-flow exchange at the boundary between fracture and matrix is short with respect to the residence time of water in the fracture. Hence, the water cut is small.
- At high Peclet numbers, the convective transport is dominant over imbibition and hence the oil recovery mechanism is limited by the rate of imbibition. Furthermore, the residence time of water is much shorter than the characteristic time of imbibition. As a result, less fluid-flow exchange occurs for the same amount of injected water. Thus, if we were in the high-Peclet-number regime, the water cut is large.

Effects of contact angles, mixed wetting, and non-equilibrium effects on oil recovery:

- At low Peclet numbers and high gravity numbers, gravity segregation is more pronounced at high contact angles, because for large contact angles the mixing tendency by capillary forces is reduced. In the absence of gravity, the difference between oil recoveries for different contact angles is small. On the other hand, for large Peclet numbers, the production after water breakthrough appears to be more or less proportional to  $\cos \theta$ . As a result, the effect of contact angle on oil recovery is more pronounced.
- The recovery for mixed-wet is less than for the finite contact angle water-wet case.
- The recovery for the mixed-wet fracture/mixed-wet matrix case is higher than for the water-wet fracture/mixed-wet matrix case at low Peclet numbers because of a combination of capillary imbibition and gravity drainage. However, at large Peclet numbers and thus low gravity numbers, the recovery for both cases appears to be the same.
- Waterflooding in completely oil-wet fractured reservoirs results in a poor recovery, in particular at large Peclet numbers.
- For low Peclet numbers, the ultimate oil recovery for water-wet fracture/mixed-wet matrix fractured reservoirs is reached faster than for high Peclet numbers and is about the matrix Amott index times the recovery obtained with completely water-wet reservoirs. Nonetheless, for large Peclet numbers, the recovery ratio ( $\Xi$ ) is smaller than the matrix Amott index.
- If the residence time of water in the fractured reservoir is much longer than the delay time  $\tau$ , the delay time (non-equilibrium effects) does not influence oil recovery qualitatively. Conversely, for large Peclet numbers, the residence time of water in the fractures is short and hence high values of  $\tau$  significantly slow down the oil recovery due to the non-equilibrium effects.

It is asserted that in partially water-wet systems, the values of the delay time  $\tau$  can be long (of the order of 100 days) due to the fact that first an oil film must be removed from the corrugated surface of the grains by a combined dissolution/diffusion process.

Experiments in the laboratory are expected to be more sensitive to non-equilibrium capillary-pressure effects as Peclet numbers are usually high. The delay time  $\tau$  can easily exceed the experimentation time. It is important to distinguish between truly oil-wet systems and systems that are water-wet with long delay times.

In view of the transparent physical basis of homogenization, we assert that improved fracture modeling can be achieved using the upscaled-VFR model.

## Acknowledgment

We thank Statoil-Hydro for supporting our research on oil recovery from fractured reservoirs. We also thank Sharif University of Technology for their steady collaboration and the National Iranian Oil Company (NIOC) for continuous support of this work. We acknowledge Maryam Namdar Zanganeh, William R. Rossen, Stefan M. Luthi, and Giovanni Bertotti for many useful discussions and comments. We also acknowledge SPE for granting the Nico van Wingen Memorial Graduate Fellowship in Petroleum Engineering to the first author.

## Nomenclature

$A$	= horizontal cross-section
$B$	= 3D domain
$\mathbf{c}$	= vector of the matrix-cell center
$d$	= size of a grid cell
$D_{cap}$	= capillary-diffusion coefficient

<b>e</b>	= unit normal vector
<i>F</i>	= nonlinear fracture function
<i>F</i> <sub>1,2</sub>	= fracture set
<i>g</i>	= gravity acceleration
<i>H</i>	= height of the reservoir, L, m
<i>I</i> <sub>w</sub>	= Amott index
<b>I</b>	= unit tensor
<i>k</i>	= permeability, L <sup>2</sup> , mD
<i>K</i>	= effective fracture permeability, L <sup>2</sup> , mD
<i>k<sub>r</sub></i>	= relative permeability
<i>l</i>	= local scale (lateral matrix-column size)
<i>L</i>	= global scale / length of the reservoir, L, m
<i>M</i>	= nonlinear matrix function
<b>n</b>	= unit normal vector
<i>N<sub>f</sub></i>	= number of fracture grid cells
<i>N<sub>G</sub></i>	= gravity number
<i>N<sub>m</sub></i>	= number of matrix grid cells
<i>N<sub>zf</sub></i>	= number of fracture grid cells in the vertical direction
<b>p</b>	= vector of the fracture-cell center
<i>P</i>	= pressure, m/Lt <sup>2</sup> , MPa
<i>p<sub>c</sub></i>	= capillary pressure, m/Lt <sup>2</sup> , kPa
<b>p'</b>	= vector of the fracture-cell center on a horizontal cross-section
<i>Pe</i>	= peclet number
<i>PV</i>	= pore volume
<b>q</b>	= any parameter
<i>Q</i>	= 3D domain
<i>q<sub>ext</sub></i>	= water injection rate, PV/yr
<b>r</b>	= coordinate vector
<i>R</i>	= real
<i>S</i>	= saturation
<i>S<sub>ir,w</sub></i>	= irreducible water saturation
<i>S<sub>or</sub></i>	= residual oil saturation
<i>SU</i>	= small unit
<i>t</i>	= time, t, sec
<i>u</i>	= velocity
<b>u</b>	= velocity vector
<i>W</i>	= width of the reservoir, L, m
<i>x</i>	= x-coordinate
<b>x<sub>b</sub></b>	= global coordinate
<b>x<sub>p</sub></b>	= center of a grid cell
<b>x<sub>s</sub></b>	= local coordinate
<i>x'</i>	= horizontal cross-section position
<i>y</i>	= y-coordinate
<i>z</i>	= vertical upward direction
<i>Z</i>	= 1D domain
<b>Greek</b>	
<i>α</i>	= phase (oil / water)
<i>ε</i>	= scaling ratio
<i>η</i>	= effective water saturation
<i>θ</i>	= contact angle
<i>λ</i>	= mobility
<i>μ</i>	= viscosity, m/Lt, cp
<i>ξ</i>	= potential / Saturation indicator
<i>Ξ</i>	= recovery ratio
<i>ρ</i>	= density, m/L <sup>3</sup> , kg/m <sup>3</sup>
<i>σ</i>	= coordinates of the boundary
<i>τ</i>	= delay time, t, sec
<i>φ</i>	= porosity
<b>Φ</b>	= potential
<b>Ω</b>	= horizontal cross-section domain

$\omega$  = auxiliary function

### Math Signs and Operators

$\langle \rangle$  = average sign over volume

$||$  = absolute value of volume

$\approx$  = almost equal to

$\otimes$  = dyadic product

$\sqrt{\quad}$  = square root

$\int$  = integral

$\rightarrow$  = vector sign

$d$  = differential

$\partial_{\pi}$  = partial differential with respect to  $\pi$

$\partial$  = boundary of

$\nabla$  = del (gradient operator)

$\Delta$  = delta (difference operator)

$\nabla \cdot$  = divergence operator

### Subscripts

$b$  = global (big) index

$D$  = dimensionless

$f$  = fracture

$m$  = matrix

$o$  = oil phase

$r$  = relative

$R$  = reference

$s$  = local (small) index

$w$  = water phase

$z$  = z-coordinate (vertical direction)

$\alpha$  = oil/water index

$\zeta$  = fracture/matrix index

### Superscripts

\* = local fracture index

### References

- Aguilera, R. 1998. Geological Aspects of Naturally Fractured Reservoirs. *The Leading Edge* **17** (12): 1667-1670.
- Al-Harbi, M., Cheng, H., He, Z., and Datta-Gupta, A. 2005. Streamline-Based Production Data Integration in Naturally Fractured Reservoirs. *SPE J.* **10** (4): 426-439.
- Al-Huthali, A. and Datta-Gupta, A. 2004. Streamline Simulation of Counter-Current Imbibition in Naturally Fractured Reservoirs. *J. Pet. Sci. Eng.* **43** (3-4): 271-300.
- Anderson, W.G. 1987. Wettability Literature Survey-Part 6: The Effects of Wettability on Waterflooding. *J. Pet. Tech* **39** (12): 1605-1622.
- Arbogast, T. 1993. Gravitational Forces in Dual-Porosity Systems: I. Model Derivation by Homogenization. *Transp. Porous Media* **13** (2): 179-203.
- Arbogast, T. 1997. Computational Aspects of Dual-Porosity Models. In *Homogenization and Porous Media, Interdisciplinary Applied Mathematics*, 6th edn, ed. U. Hornung, pp. 203-223. New York: Springer.
- Auriault, J.-L. and Lewandowska, J. 1996. Diffusion/Adsorption/Advection Macrotransport in Soils. *European Journal of Mechanics, A/Solids* **15** (4): 681-704.
- Balogun, A., Kazemi, H., Ozkan, E., Al-Kobaisi, M., and Ramirez, B. 2009. Verification and proper Use of Water-Oil Transfer Function for Dual-Porosity and Dual-Permeability Reservoirs. *SPE Res Eval & Eng* **12** (2): 189-199. SPE-104580-PA.
- Barenblatt, G.I., Zheltov, Iu.P., and Kochina, I.N. 1960. Basic Concept in the Theory of Seepage of Homogeneous Liquids in Fissured Rocks. *J. of Applied Mathematics and Mechanics* **24** (5): 1286-1303.
- Barenblatt, G.I. 1971. Filtration of Two Nonmixing Fluids in a Homogeneous Porous Medium. *Soviet Academy Izvestia. Mechanics of Gas and Fluids* **5**: 857-864.
- Barenblatt, G.I. and Gilman, A.A. 1987. Nonequilibrium Counterflow Capillary Impregnation. *J. Eng. Phys.* **52** (3): 335-339.
- Barenblatt, G.I., Garcia-Azorero, J., De Pablo, A., and Vazquez, J.L. 1997. Mathematical Model of the Non-Equilibrium Water-Oil Displacement in Porous Strata. *Applicable Analysis* **65**: 19-45.
- Barenblatt, G.I., Patzek, T.W., and Silin, D.B. 2003. The mathematical Model of Nonequilibrium Effects in Water-Oil Displacement. *SPE J.* **8** (4): 409-416. SPE-87329-PA.
- Behbahani, H. and Blunt, M.J. 2005. Analysis of Imbibition in Mixed-Wet Rocks Using Pore-Scale Modeling. *SPE J.* **10** (4): 466-473. SPE-90132-PA.
- Dahan, O., Nativ, R., Adar, E., and Berkowitz, B. 1998. A Measurement System to Determine Water Flux and Solute Transport through Fractures in the Unsaturated Zone. *Ground Water* **36** (3): 444-449.
- Delshad, M. Fathi Najafabadi, N., Anderson, G.A., and Pope, G.A. 2009. Modeling Wettability Alteration by Surfactants in Naturally Fractured Reservoirs. *SPE Res Eval Eng* **12** (3): 361-370. SPE-100081-PA.
- Douglas, J. Jr., Hensley, J.L., and Arbogast, T. 1991. A Dual-Porosity Model for Waterflooding in Naturally Fractured Reservoirs. *Comput. Meth. Appl. Mech. Eng.* **87** (2-3): 157-174.

- Elzeftawy, A. and Mansell, R.S. 1975. Hydraulic Conductivity Calculations for Unsaturated Steady-State and Transient-State Flow in Sands. *Soil Sci. Soc. Am. Proc.* **39**: 599-603.
- Finkbeiner, T., Barton, C.A., and Zoback, M.D. 1997. Relationships among In-Situ Stress, Fractures and Faults, and Fluid Flow: Monterey Formation, Santa Maria Basin, California. *American Association of Petroleum Geologists Bulletin* **81** (12): 1975-1999.
- Firoozabadi, A. 2000. Recovery Mechanisms in Fractured Reservoirs and Field Performance. *J. Cdn. Pet. Tech.* **39** (11): 13-17.
- Fischer, H. and Morrow, N.R. 2006. Scaling of Oil Recovery by Spontaneous Imbibition for Wide Variation in Aqueous Phase Viscosity with Glycerol as the Viscosifying Agent. *J. Pet. Sci. Eng.* **52** (1-4): 35-53.
- Fischer, H., Wo, S., and Morrow, N.R. 2008. Modeling the Effect of Viscosity Ratio on Spontaneous Imbibition. *SPE Res Eval & Eng* **11** (3): 577-589. SPE-102641-PA
- Graue, A., Bognø, T., Baldwin, B.A., and Spinler, E.A. 2001. Wettability Effects on Oil-Recovery Mechanisms in Fractured Reservoirs. *SPE Res Eval & Eng* **4** (6): 455-465. SPE-74335-PA.
- Hassanizadeh, S.M. and Gray, W.G. 1990. Mechanics and Thermodynamics of Multiphase Flow in Porous Media Including Interphase Boundaries. *Adv. Water Resour.* **13** (4): 169-186.
- Hassanizadeh, S.M. and Gray, W.G. 1993. Thermodynamic Basis of Capillary Pressure in Porous Media. *Water Resour. Res.* **29** (10): 3389-3405.
- Hassanizadeh, S.M., Celia, M.A., and Dahle, H.K. 2002. Dynamic Effect in the Capillary Pressure-Saturation Relationship and Its Impact on Unsaturated Flow. *Vadose Zone J.* **1**: 38-57.
- Hatiboglu, C.U. and Babadagli, T. 2007. Oil Recovery by Counter-Current Spontaneous Imbibition: Effects of Matrix Shape Factor, Gravity, IFT, Oil Viscosity, Wettability, and Rock Type. *J. Pet. Sci. Eng.* **59** (1-2): 106-122.
- Karimaie, H. and Torsæter, O. 2007. Effect of Injection Rate, Initial Water Saturation and Gravity on Water Injection in Slightly Water-Wet Fractured Porous Media. *J. Pet. Sci. Eng.* **58** (1-2): 293-308.
- Kazemi, H. 1969. The Interpretation of Interference Tests in Naturally Fractured Reservoirs with Uniform Fracture Distribution. *SPE J.* **9** (4): 451-462. SPE-2156-A.
- Kazemi, H., Gilman, J.R., and Elasharkawy, A.M. 1992. Analytical and Numerical Solution of Oil Recovery from Fractured Reservoirs with Empirical Transfer Functions. *SPE Res Eng* **7** (2): 219-227.
- Leverett, M.C. Flow of Oil-Water Mixtures through Unconsolidated Sands. 1939. *Trans.*, AIME **132**: 149-171.
- Monteagudo, J.E.P. and Firoozabadi, A. 2007. Control-Volume Model for Simulation of Water Injection in Fractured Media: Incorporating Matrix Heterogeneity and Reservoir Wettability Effects. *SPE J.* **12** (3): 355-366. SPE-98108-PA.
- Morrow, N.R. and Mason, G. 2001. Recovery of Oil by Spontaneous Imbibition. *Curr. Opin. Colloid Interface Sci.* **6** (4): 321-337.
- Muskat, M. and Meres, M.W. 1936. The Flow of Heterogeneous Fluids through Porous Media. *J. Appl. Phys.* **7** (921): 346-363.
- Nelson, R.A. 2001. *Geologic Analysis of Naturally Fractured Reservoirs*, second edition. Woburn, USA: Gulf Professional Publishing.
- Pavone, D.R. 1990. A Darcy's Law Extension and a New Capillary Pressure Equation for Two-Phase Flow in Porous Media. Paper SPE 20474 presented at the SPE Annual Technical Conference and Exhibition, New Orleans, Louisiana, 23-26 September. SPE-20474-MS.
- Plug, W.J. and Bruining, J. 2007. Capillary Pressure for the Sand-CO<sub>2</sub>-Water System under Various Pressure Conditions. Application to CO<sub>2</sub> Sequestration. *Adv. Water Resour.* **30** (11): 2339-2353.
- Plug, W.J., Mazumder, S., and Bruining, J. 2008. Capillary Pressure and Wettability Behavior of CO<sub>2</sub> Sequestration in Coal at Elevated Pressures. *SPE J.* **13** (4): 455-464. SPE-108161-PA.
- Pooladi-Darvish, M. and Firoozabadi, A. 2000. Cocurrent and Countercurrent Imbibition in a Water-Wet Matrix Block. *SPE J.* **5** (1): 3-11. SPE-38443-PA.
- Punternvold, T. and Austad, T. 2008. Injection of Seawater and Mixtures with Produced Water into North Sea Chalk Formation: Impact of Fluid-Rock Interactions on Wettability and Scale Formation. *J. Pet. Sci. Eng.* **63** (1-4): 23-33.
- Punternvold, T., Strand, S., and Austad, T. 2009. Coinjection of Seawater and Produced Water to Improve Oil Recovery from Fractured North Sea Chalk Oil Reservoirs. *Energy and Fuels* **23** (5): 2527-2536.
- Rangel-German, E.R. and Kovscek, A.R. 2002. Experimental and Analytical Study of Multidimensional Imbibition in Fractured Porous Media. *J. Pet. Sci. Eng.* **36** (1-2): 45-60.
- Saidi, A.M. 1983. Simulation of Naturally Fractured Reservoirs. Paper SPE 12270 presented at the SPE Reservoir Simulation Symposium, San Francisco, California, 15-18 November.
- Salimi, H. and Bruining, J. 2008. Improved Prediction of Oil Recovery from Waterflooded Fractured Reservoirs. Paper SPE 115361 presented at the SPE Annual Technical Conference and Exhibition, Denver, Colorado, 21-24 September. doi: 10.2118/115361-MS.
- Salimi, H. and Bruining, J. 2009. Upscaling in Partially Fractured Oil Reservoirs Using Homogenization. Paper SPE 125559 presented at the SPE/EAGE Reservoir Characterization and Simulation Conference, Abu Dhabi, UAE, 19-21 October. doi: 10.2118/125559-MS.
- Salimi, H. and Bruining, J. 2010a. Improved Prediction of Oil Recovery from Waterflooded Fractured Reservoirs Using Homogenization. *SPE Res Eval & Eng* **13** (1): 44-55. SPE-115361-PA. doi: 10.2118/115361-PA.
- Salimi, H. and Bruining, H. 2010b. Upscaling in Vertically Fractured Oil Reservoirs Using Homogenization. *Transp. Porous Media* **84** (1): 21-53. doi: 10.1007/s11242-009-9483-1.
- Salimi, H. and Bruining, J. 2010c. The Influence of Heterogeneity, Wettability, and Viscosity Ratio on Oil Recovery from Vertically Fractured Oil Reservoirs. Accepted for publication in *SPE Journal*. SPE-140152-PA. doi: 10.2118/140152-PA.
- Salimi, H. and Bruining, J. 2010d. Upscaling of Fractured Oil Reservoirs Using Homogenization Including Non-Equilibrium Capillary Pressure. Paper A001 presented at the 12<sup>th</sup> European Conference on the Mathematics of Oil Recovery (ECMOR), Oxford, UK, 6-9 September.
- Sarma, P. and Aziz, K. 2006. New Transfer Function for Simulation of Naturally Fractured Reservoirs with Dual-Porosity Models. *SPE J.* **11** (3): 328-340.
- Seethapalli, A., Adibhatla, B., and Mohanty, K.K. 2004. Physicochemical Interactions During Surfactants Flooding of Fractured Carbonate Reservoirs. *SPE J.* **9** (4): 411-418. SPE-89423-PA.
- Shook, M., Li, D., and Lake, L.W. 1992. Scaling Immiscible Flow through Permeable Media by Inspectional Analysis. *In SITU* **16** (4): 311-349.

- Siemons, N., Bruining, J., Castelijns, H., and Wolf, K.H. 2006. Pressure Dependence of the Contact Angle in a CO<sub>2</sub>-H<sub>2</sub>O-Coal System. *J. Colloid Interface Sci.* **297** (2): 755-761.
- Smiles, D.E., Vachaud, G., and Vauclin, M. 1971. A Test of the Uniqueness of the Soil Moisture Characteristic During Transient, Non-Hysteretic Flow of Water in a Rigid Soil. *Soil Sci. Soc. Am. Proc.* **35**: 535-539.
- Sonier, F., Souillard, P., and Blaskovich, F.T. 1988. Numerical Simulation of Naturally Fractured Reservoirs. *SPE Res Eng* **3** (4): 1114-1122.
- Stauffer, F. 1978. Time Dependence of the Relations Between Capillary Pressure, Water Content and Conductivity During Drainage of Porous Media. IAHR Symposium on Scale Effects in Porous Media, Thessaloniki, Greece, 29 August-1 September.
- Tang, G-Q. and Firoozabadi, A. 2001. Effect of Pressure Gradient and Initial Water Saturation on Water Injection in Water-Wet and Mixed-Wet Fractured Porous Media. *SPE Res Eval & Eng* **4** (6): 516-524. SPE-74711-PA.
- Tartakovsky, A. and Meakin, P. 2005. Modeling of Surface Tension and Contact Angles with Smoothed Particle Hydrodynamics. *Phys. Rev. E* **72** (2): 1-9. art. no. 026301.
- Teixell, A., Durney, D.W., and Arboleya, M.L. 2000. Stress and Fluid Control on Decollement within Competent Limestone. *Journal of Structural Geology* **22** (3): 349-371.
- Tong, Z., Xie, X., and Morrow, N.R. 2002. Scaling for Viscosity Ratio for Oil Recovery by Imbibition from Mixed-Wet Rocks. *Petrophysics* **43** (4): 338-346.
- Topp, G.C., Klute, A., and Peters, D.B. 1967. Comparison of Water Content-Pressure Head Data Obtained by Equilibrium, Steady-State and Unsteady-State Methods. *Soil Sci. Soc. Am. Proc.* **31**: 312-314.
- Vachaud, G., Vauclin, M., and Wakil, M. 1972. A Study of the Uniqueness of the Soil Moisture Characteristic During Desorption by Vertical Drainage. *Soil Sci. Soc. Am. Proc.* **36**: 531-532.
- Van Duijn, C.J., Molenaar, J. and Neef, M.J. 1995. The Effect of Capillary Forces on Immiscible Two-Phase Flow in Heterogeneous Porous Media. *Transp. Porous Media* **21** (1): 71-93.
- Warren, J.E. and Root, P.J. 1963. The Behavior of Naturally Fractured Reservoirs. *SPE J.* **3** (3): 245-255; *Trans.*, AIME, **228**. SPE-426-PA.
- Wu, Y.S., Pan, L., and Pruess, K. 2004. A Physically Based Approach for Modeling Multiphase Fracture-Matrix Interaction in Fractured Porous Media. *Adv. Water Resour.* **27** (9): 875-887.
- Yortsos, Y.C. 1991. A Theoretical Analysis of Vertical Flow Equilibrium. Paper SPE 22612 presented at the SPE Annual Technical Conference and Exhibition, Dallas, Texas, 6-9 October.
- Yu, L., Evje, S., Kleppe, H., Karstad, T., Fjelde, I., and Skjaeveland, S.M. 2009. Spontaneous Imbibition of Seawater into Preferentially Oil-Wet Chalk Cores-Experiments and Simulations. *J. Pet. Sci. Eng.* **66** (3-4): 171-179.
- Zanini, L., Novakowski, K.S., Lapcevic, P., Bickerton, G.S., Voralek, J., and Talbot, C. 2000. Ground Water Flow in a Fractured Carbonate Aquifer Inferred from Combined Hydrogeological and Geochemical Measurements. *Ground Water* **38** (3): 350-360.

#### Appendix A—Numerical Solution For The Upscaled-VFR Model Including Non-Equilibrium Effects

The numerical procedure described below is an extension of the method used by Arbogast (1997), Salimi and Bruining (2010a) for the sugar-cube model, and by Salimi and Bruining (2010b) for the upscaled-VFR model without non-equilibrium effects. The difficulty arises due to a coupling of flow in the vertical direction, which is important in the upscaled-VFR model. From the computational point of view, we consider a matrix column associated with each point in the base plane of the reservoir. The horizontal cross-sectional position of any point  $\mathbf{r}_b = (x_b, y_b, z_b) \in Q$ , is denoted by  $\mathbf{r}'_b = (x_b, y_b) \in A_Q$ . The matrix column at  $\mathbf{r}'_b = (x_b, y_b) \in A_Q$  is denoted by  $B_m(\mathbf{r}'_b) = \Omega_m(\mathbf{r}'_b) \times H$ , where this matrix column is representative of matrix columns in the vicinity of  $\mathbf{r}'$ . We formulate our numerical method in terms of the water potential, the capillary pressure, and the water saturation. Here, we also define the capillary potential  $\Phi_c = P_c + (\rho_o - \rho_w)gz$ . We assume that all external sources, i.e., the production and injection wells, influence only the fractures. Eqs. 11 and 15 above are called the saturation equations, and the sums over the phases of each of the two-phase equations are Eqs. 12 and 16, the pressure equations.

Initially, there is capillary-gravity equilibrium both in the fracture system and in the matrix column. This means that the fluid-exchange term between fracture and matrix is zero initially. In addition, the effective water saturation  $\eta$  is equal to the actual water saturation  $S_w$  for Barenblatt's approach. Since initial oil-in-place is known, we determine the initial fracture water potential by solving the fracture pressure equation (Eq. 12). Because of equilibrium, we can solve the matrix pressure equation (Eq. 16) to obtain the initial matrix water potential.

Equations 9 through 18 cannot be solved sequentially or explicitly, because a small change in the boundary values on each matrix column can cause flow of a volume of fluid that is large in comparison to the volume of the fractures (Douglas et al. 1991). In other words, the matrix absorbs more fluid from the surrounding fractures in one step than can be resident there. Part of the excess volume in the matrix is returned to the fractures in the next step, however, violating mass conservation. Therefore, the fracture-matrix interaction must be handled implicitly.

We use a backward-Euler time approximation for the complete system of Eqs. 9, and 11 through 18. We further use a finite-volume approach and first-order upwind scheme for spatial discretization. To facilitate the implementation of the no-flow boundary conditions and the continuity conditions of the potentials along the fracture-matrix interfaces, we discretize the space variables in a cell-centered manner in the fractures and also cell-centered with respect to  $z$  in the matrix columns. However, the discretization in the  $x_s$  and  $y_s$  are vertex-centered. In this work, we use uniform grid cells in the fractures and in each matrix column. From the computational perspective, we consider a case in which the vertical discretization in the matrix columns coincides with that in the fractures.

We discretize  $Q$  into  $N_{xf} \times N_{yf} \times N_{zf}$  grid cells, each grid cell of size  $d_{xf} \times d_{yf} \times d_{zf}$ . The center of the fracture-cell  $\mathbf{p} = (p_x, p_y, p_z)$  is then

$$\mathbf{x}_{bp} = \left( (p_x - 1/2)d_{xf}, (p_y - 1/2)d_{yf}, (p_z - 1/2)d_{zf} \right), \quad (\text{A-1})$$

and the set of all fracture grid cell centers is

$$N_f = \{ \mathbf{x}_{bp_i} : p_i = 1, 2, 3, \dots, N_{if}, i = x, y, z \}. \quad (\text{A-2})$$

This reduces the system of the equations to a fully discrete, three-dimensional problem. We denote the vectors of unknowns in the fracture by

$$\begin{aligned} \bar{\Phi}_{wf}^n &= \{ \Phi_{wf,i}^n, i = 1, 2, 3, \dots, N_{xf} \times N_{yf} \times N_{zf} \}, \\ \bar{S}_{wf}^n &= \{ S_{wf,i}^n, i = 1, 2, 3, \dots, N_{xf} \times N_{yf} \times N_{zf} \}, \end{aligned} \quad (\text{A-3})$$

where superscript  $n$  denotes the time level  $n$ . In the vector, the potentials and saturations are stacked behind each other. At each  $\mathbf{x}_{bp} \in N_f$ , there is a representative matrix column  $B_m(\mathbf{x}_{bp}) = (0, d_{xm} N_{xm}) \times (0, d_{ym} N_{ym}) \times (0, d_{zf} N_{zf})$ , where  $\mathbf{p}' = (p_x, p_y)$  is the projection of  $\mathbf{p}$  on the  $x$ - $y$  plane. Then, the center point of each matrix cell  $\mathbf{c} = (c_x, c_y, c_z)$  is

$$\mathbf{x}_{sp'} = (c_x d_{xm, p'}, c_y d_{ym, p'}, (c_z - 1/2)d_{zf}), \quad (\text{A-5})$$

and the set of all matrix-cell-center points at fracture point  $\mathbf{p}$  is given by

$$N_{m,p'} = \{ \mathbf{x}_{sp', c_i} : c_i = 0, 1, \dots, N_{im, p'}, i = x, y; c_z = 1, 2, \dots, N_{zf} \}. \quad (\text{A-6})$$

Then, associated with each grid point  $i = 1, 2, \dots, N_{xf} \times N_{yf} \times N_{zf}$ , we have three series of matrix unknowns

$$\begin{aligned} \bar{\Phi}_{wm, i'}^n &= \{ \Phi_{wm, i'j}^n, i' = 1, 2, \dots, N_{xf} \times N_{yf}, j = 1, 2, 3, \dots, N_{xm} \times N_{ym} \times N_{zf} \}, \\ \bar{S}_{wm, i'}^n &= \{ S_{wm, i'j}^n, i' = 1, 2, \dots, N_{xf} \times N_{yf}, j = 1, 2, 3, \dots, N_{xm} \times N_{ym} \times N_{zf} \}, \\ \bar{\eta}_{wm, i'}^n &= \{ \eta_{wm, i'j}^n, i' = 1, 2, \dots, N_{xf} \times N_{yf}, j = 1, 2, 3, \dots, N_{xm} \times N_{ym} \times N_{zf} \}, \end{aligned} \quad (\text{A-7})$$

in the  $m^{\text{th}}$  matrix column. After that, we can write the fully discrete, nonlinear fracture and matrix equations

$$\begin{cases} F_i(\bar{\Phi}_{wf}^n, \bar{S}_{wf}^n, \bar{\Phi}_{wm}^n, \bar{S}_{wm}^n) = 0, & i = 1, 2, \dots, N_{xf} \times N_{yf} \times N_{zf}, \\ M_{i'j}(\bar{\Phi}_{wf}^n, \bar{S}_{wf}^n, \bar{\Phi}_{wm, i'}^n, \bar{S}_{wm, i'}^n, \bar{\eta}_{wm, i'}^n) = 0, & \begin{cases} i' = 1, 2, \dots, N_{xf} \times N_{yf}, \\ j = 1, 2, \dots, N_{xm} \times N_{ym} \times N_{zf}, \end{cases} \end{cases} \quad (\text{A-8})$$

where  $F_i$  and  $M_{i'j}$  are some nonlinear functions. We use Newton's method to linearize the above system of equations. Let

$$\bar{\Phi}_{wf}^{n,k}, \bar{S}_{wf}^{n,k}, \bar{\Phi}_{wm}^{n,k}, \bar{S}_{wm}^{n,k} \text{ and } \bar{\eta}_{wm}^{n,k}, \quad (\text{A-9})$$

denote the  $k^{\text{th}}$  Newton iteration for the  $n^{\text{th}}$  time level's solution. We write the evaluation of  $F$  and  $M$  at the  $(k-1)^{\text{th}}$  iteration for the  $n^{\text{th}}$  time level solution as

$$\begin{cases} F_i^{n,k-1} = F_i(\bar{\Phi}_{wf}^{n,k-1}, \bar{S}_{wf}^{n,k-1}, \bar{\Phi}_{wm}^{n,k-1}, \bar{S}_{wm}^{n,k-1}), \\ M_{i'j}^{n,k-1} = M_{i'j}(\bar{\Phi}_{wf}^{n,k-1}, \bar{S}_{wf}^{n,k-1}, \bar{\Phi}_{wm, i'}^{n,k-1}, \bar{S}_{wm, i'}^{n,k-1}, \bar{\eta}_{wm, i'}^{n,k-1}). \end{cases} \quad (\text{A-10})$$

Let  $\partial_\pi$  denote the partial derivative with respect to  $\pi$ . We will develop an efficient numerical scheme based on the conventional Newton procedure. Such a conventional procedure would run as follows:

(1) Start with an initial guess for the solution

$$\bar{\Phi}_{wf}^{n,0}, \bar{S}_{wf}^{n,0}, \bar{\Phi}_{wm}^{n,0}, \bar{S}_{wm}^{n,0}, \text{ and } \bar{\eta}_{wm}^{n,0}. \quad (\text{A-11})$$

Note that we use the initial water potential and water saturation as a first guess for the Newton iteration of the first time step. The initial capillary potentials  $\Phi_c$  in the fracture system and in the matrix column should agree on the matrix column boundary, i.e., continuity of capillary pressure.

(2) For each  $k = 1, 2, \dots, n$  until convergence is reached:

(a) Solve for

$$\bar{\Phi}_{wf}^{n,k}, \bar{S}_{wf}^{n,k}, \bar{\Phi}_{wm}^{n,k}, \bar{S}_{wm}^{n,k}, \text{ and } \bar{\eta}_{wm}^{n,k},$$

satisfying

$$\begin{cases}
F_i^{n,k-1} + \sum_{i'=1}^{N_f} \left[ \partial_{\Phi_{wf,i'}} F_i^{n,k-1} \delta\Phi_{wf,i'}^{n,k} + \partial_{S_{wf,i'}} F_i^{n,k-1} \delta S_{wf,i'}^{n,k} \right] + \\
+ \sum_{j'=1}^{N_m} \left[ \partial_{\Phi_{wm,i'j'}} F_i^{n,k-1} \delta\Phi_{wm,i'j'}^{n,k} + \partial_{S_{wm,i'j'}} F_i^{n,k-1} \delta S_{wm,i'j'}^{n,k} + \partial_{\eta_{wm,i'j'}} F_i^{n,k-1} \delta\eta_{wm,i'j'}^{n,k} \right] = 0, \quad i = 1, 2, \dots, N_f, \\
M_{ij}^{n,k-1} + \sum_{l=1}^{N_f} \left[ \partial_{\Phi_{wf,(i,l)}} M_{ij}^{n,k-1} \delta\Phi_{wf,(i,l)}^{n,k} + \partial_{S_{wf,(i,l)}} M_{ij}^{n,k-1} \delta S_{wf,(i,l)}^{n,k} \right] + \\
+ \sum_{j'=1}^{N_m} \left[ \partial_{\Phi_{wm,i'j'}} M_{ij}^{n,k-1} \delta\Phi_{wm,i'j'}^{n,k} + \partial_{S_{wm,i'j'}} M_{ij}^{n,k-1} \delta S_{wm,i'j'}^{n,k} + \partial_{\eta_{wm,i'j'}} M_{ij}^{n,k-1} \delta\eta_{wm,i'j'}^{n,k} \right] = 0,
\end{cases} \quad \begin{cases}
i' = 1, 2, \dots, N_{xf} \times N_{yf}, \\
j = 1, 2, \dots, N_m.
\end{cases} \quad (\text{A-12})$$

(b) Update the potential and saturations

$$\begin{aligned}
\bar{\Phi}_{wf}^{n,k} &= \bar{\Phi}_{wf}^{n,k-1} + \delta\bar{\Phi}_{wf}^{n,k}, & \bar{S}_{wf}^{n,k} &= \bar{S}_{wf}^{n,k-1} + \delta\bar{S}_{wf}^{n,k}, \\
\bar{\Phi}_{wm}^{n,k} &= \bar{\Phi}_{wm}^{n,k-1} + \delta\bar{\Phi}_{wm}^{n,k}, & \bar{S}_{wm}^{n,k} &= \bar{S}_{wm}^{n,k-1} + \delta\bar{S}_{wm}^{n,k}, & \bar{\eta}_{wm}^{n,k} &= \bar{\eta}_{wm}^{n,k-1} + \delta\bar{\eta}_{wm}^{n,k}.
\end{aligned} \quad (\text{A-13})$$

This would complete the algorithm for a time step. The above linear system (Eq. A-12) involves the solution of a  $(2 \times N_f + 3 \times N_{xf} \times N_{yf} \times N_m) \times (2 \times N_f + 3 \times N_{xf} \times N_{yf} \times N_m)$  matrix for each Newton iteration at a time step, which is computationally expensive. Within the linearized Newton problem (Eq. A-12), the matrix solutions in the  $i^{\text{th}}$  column depend on  $\Phi_{wf,(i,l)}^{n,k}$  and  $S_{wf,(i,l)}^{n,k}$ , where  $l=1, 2, \dots, N_{zf}$ . In other words, the matrix solution in the  $i^{\text{th}}$  column only depends on all the fracture cells surrounding the matrix column of interest. It is therefore possible to develop an efficient numerical scheme by decoupling the matrix and fracture problems without affecting the implicit nature of the scheme. We replace the matrix problem in Eq. A-12 by the following three types of problems for

$$\left( \delta\bar{\Phi}_{wm,(i,l)}^{n,m}, \delta\bar{S}_{wm,(i,l)}^{n,m}, \delta\bar{\eta}_{wm,(i,l)}^{n,m} \right), \quad \left( \hat{\delta}\bar{\Phi}_{wm,(i,l)}^{n,m}, \hat{\delta}\bar{S}_{wm,(i,l)}^{n,m}, \hat{\delta}\bar{\eta}_{wm,(i,l)}^{n,m} \right), \quad \text{and} \quad \left( \bar{\delta}\bar{\Phi}_{wm,i'}^{n,m}, \bar{\delta}\bar{S}_{wm,i'}^{n,m}, \bar{\delta}\bar{\eta}_{wm,i'}^{n,m} \right),$$

where  $\delta\bar{\cdot}$ 's,  $\hat{\delta}\bar{\cdot}$ 's, and  $\bar{\delta}\bar{\cdot}$ 's satisfy three types of problems as follows:

Firstly, for each  $i' = 1, 2, \dots, N_{xf} \times N_{yf}$  and  $j = 1, 2, 3, \dots, N_m$ ,

$$M_{ij}^{n,k-1} + \sum_{j'=1}^{N_m} \left[ \partial_{\Phi_{wm,i'j'}} M_{ij}^{n,k-1} \delta\bar{\Phi}_{wm,i'j'}^{n,k} + \partial_{S_{wm,i'j'}} M_{ij}^{n,k-1} \delta\bar{S}_{wm,i'j'}^{n,k} + \partial_{\eta_{wm,i'j'}} M_{ij}^{n,k-1} \delta\bar{\eta}_{wm,i'j'}^{n,k} \right] = 0, \quad (\text{A-14})$$

secondly, for  $l = 1, 2, \dots, N_{zf}$ ,

$$\partial_{\Phi_{wf,(i,l)}} M_{ij}^{n,k-1} + \sum_{j'=1}^{N_m} \left[ \partial_{\Phi_{wm,i'j'}} M_{ij}^{n,k-1} \tilde{\delta}\Phi_{wm,(i,l),j'}^{n,k} + \partial_{S_{wm,i'j'}} M_{ij}^{n,k-1} \tilde{\delta}S_{wm,(i,l),j'}^{n,k} + \partial_{\eta_{wm,i'j'}} M_{ij}^{n,k-1} \tilde{\delta}\eta_{wm,(i,l),j'}^{n,k} \right] = 0, \quad (\text{A-15})$$

thirdly, for  $l = 1, 2, \dots, N_{zf}$ ,

$$\partial_{S_{wf,(i,l)}} M_{ij}^{n,k-1} + \sum_{j'=1}^{N_m} \left[ \partial_{\Phi_{wm,i'j'}} M_{ij}^{n,k-1} \hat{\delta}\Phi_{wm,(i,l),j'}^{n,k} + \partial_{S_{wm,i'j'}} M_{ij}^{n,k-1} \hat{\delta}S_{wm,(i,l),j'}^{n,k} + \partial_{\eta_{wm,i'j'}} M_{ij}^{n,k-1} \hat{\delta}\eta_{wm,(i,l),j'}^{n,k} \right] = 0. \quad (\text{A-16})$$

If we multiply Eq. A-15 by  $\delta\Phi_{wf,(i,l)}^{n,k}$  and Eq. A-16 by  $\delta S_{wf,(i,l)}^{n,k}$  and then add these equations to Eq. A-14, the result would be identical to the matrix problem in Eq. A-12. As a result, the matrix unknowns can be calculated by

$$\delta\Phi_{wm,i'j}^{n,k} = \bar{\delta}\bar{\Phi}_{wm,i'j}^{n,k} + \sum_{l=1}^{N_{zf}} \left( \tilde{\delta}\Phi_{wm,(i,l),j}^{n,k} \delta\Phi_{wf,(i,l)}^{n,k} + \hat{\delta}\Phi_{wm,(i,l),j}^{n,k} \delta S_{wf,(i,l)}^{n,k} \right), \quad (\text{A-17})$$

$$\delta S_{wm,i'j}^{n,k} = \bar{\delta}\bar{S}_{wm,i'j}^{n,k} + \sum_{l=1}^{N_{zf}} \left( \tilde{\delta}S_{wm,(i,l),j}^{n,k} \delta\Phi_{wf,(i,l)}^{n,k} + \hat{\delta}S_{wm,(i,l),j}^{n,k} \delta S_{wf,(i,l)}^{n,k} \right), \quad (\text{A-18})$$

$$\delta\eta_{wm,i'j}^{n,k} = \bar{\delta}\bar{\eta}_{wm,i'j}^{n,k} + \sum_{l=1}^{N_{zf}} \left( \tilde{\delta}\eta_{wm,(i,l),j}^{n,k} \delta\Phi_{wf,(i,l)}^{n,k} + \hat{\delta}\eta_{wm,(i,l),j}^{n,k} \delta S_{wf,(i,l)}^{n,k} \right). \quad (\text{A-19})$$

Eqs. A-14 through A-16 can be solved independently of the fracture system. Thus, we modify step 2a of the Newton Algorithm by first solving Eqs. A-14 through A-16. The changes in the fracture unknowns are then given by solving the fracture equations of Eq. A-12, using implicitly definition of Eqs. A-17 through A-19. Subsequently, we explicitly use the changes in the fracture unknowns and Eqs. A-17 through A-19 to update the matrix  $\delta$ -potential and matrix  $\delta$ -saturation.

---

Finally, the Newton iteration can be continued. This efficient numerical method is inexpensive as it only involves the solution of many  $(3 \times N_m) \times (3 \times N_m)$  matrices and the solution of a  $(2 \times N_f) \times (2 \times N_f)$  matrix as opposed to a single big matrix. Therefore, for  $N_f = 450$  and  $N_m = 36450$  used in this paper, not only the efficient numerical method reduces the computational time approximately by a factor of 14, but also it brings roughly a saving factor of 950 in computer memory.